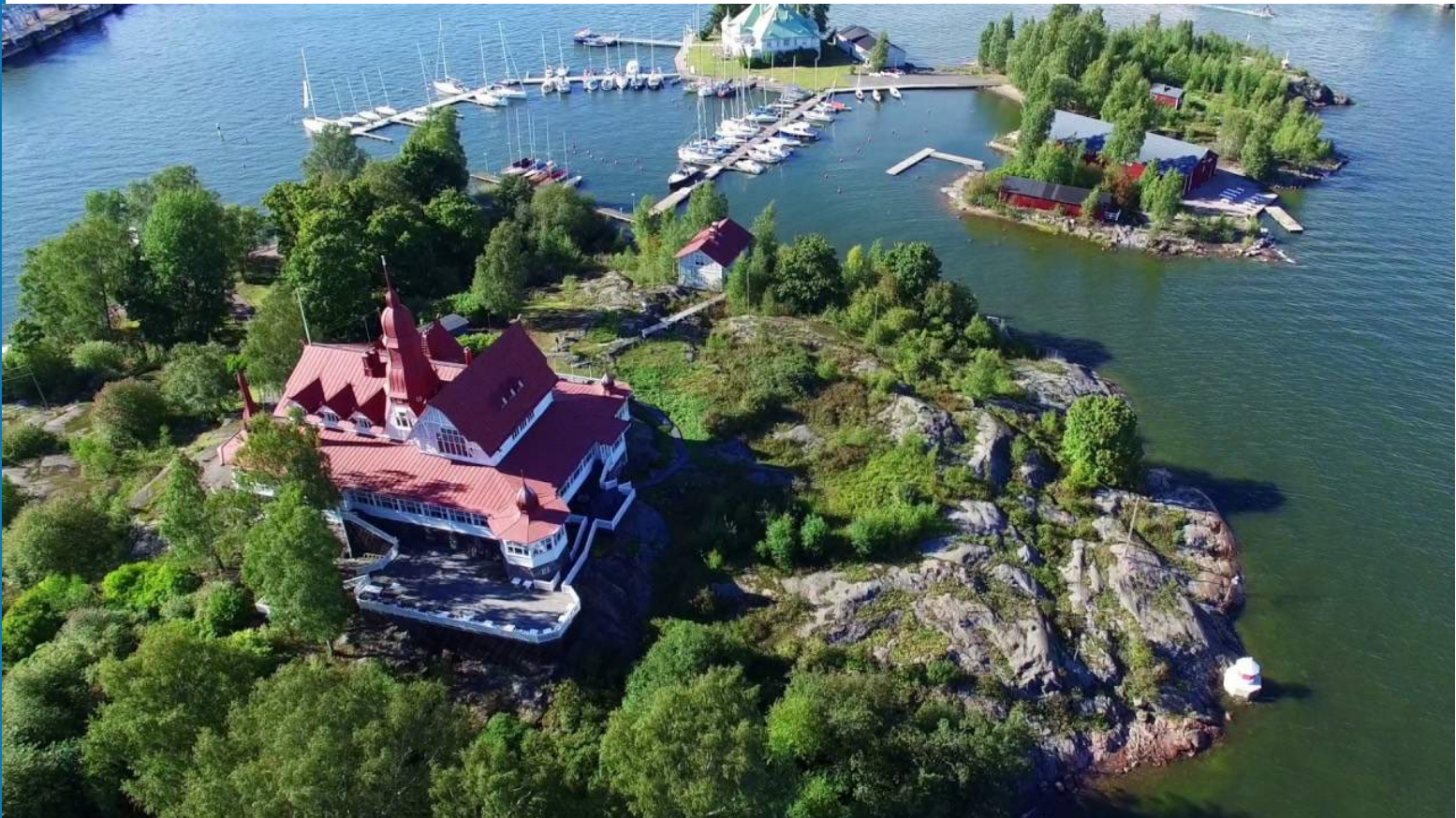




# NEWSLETTER

**In this edition:**



**Testing of a full- scale building under external blast**

**Cloud scanning and photogrammetry – a comparison of blast face surveying techniques**

**...and much more!**



10th ANNIVERSARY WORLD CONFERENCE

**HELSINKI 2019**



**10th  
ANNIVERSARY**

Scandic Marina Congress Center, Helsinki | 15th - 18th September 2019

# NEWSLETTER

## July 2019

Dear EFEE members, the President 's voice.....	3
Christer Svensson in Memoriam.....	5
Blast design and analysis from aerial imagery.....	8
Testing of a full- scale building under external blast.....	21
Cloud scanning and photogrammetry – a comparison of blast face surveying techniques....	38
PECCS - Multiplier Event in Berlin.....	53
Upcoming international and national events .....	57

We in EFEE hope you will enjoy the present EFEE-Newsletter. The next edition will be published in September 2019. Please feel free to contact the EFEE secretariat or write to [newsletter@efee.eu](mailto:newsletter@efee.eu) in case:

- You have a story you want to bring in the Newsletter
- You have a future event for the next EFEE Newsletter upcoming events list
- You want to advertise in an upcoming Newsletter edition

or any other matter.

*Doru Anghelache, Chairman of the Newsletter Committee and the Vice President of EFEE  
and Teele Tuuna, Editor of EFEE Newsletter - [newsletter@efee.eu](mailto:newsletter@efee.eu)*

*\*The articles that appear in this newsletter are the sole opinion of the authors. EFEE takes no responsibility for the accuracy or integrity of the content, and persons who rely on the content of articles do so at their own risk. EFEE encourages persons engaging in complex or hazardous activities to seek appropriate professional advice.*



EFEE SECRETARY GENERAL  
ROGER HOLMBERG, JÄRNGRUVENVÄGEN 6  
618 92 KOLMÅRDEN, SWEDEN  
[newsletter@efee.eu](mailto:newsletter@efee.eu)  
[www.efee.eu](http://www.efee.eu)

## **Dear EFEE members, the President's voice**

It is my honour to welcome you to read this summer issue of EFEE newsletter! Once again it contains several interesting technical articles and industry news.

EFEE had its Annual General Meeting in the beautiful town of Budapest in early May. All members of the previous board were selected to continue one more year in their duties. It is an honour to serve in the board of our association and I thank the EFEE council for this trust on behalf of all of us.

The board has nominated a special working group to work on the renewal of the EFEE web site. We are aiming to open the modernized site before the Helsinki Conference. Please feel free to send our secretary general all your proposals for any desired new content that you would like to see on our site in the future. We will take all proposals into consideration as we are continuously trying to improve our services and membership benefits.

The biggest EFEE event of the year is quickly approaching. Arrangements around the 10<sup>th</sup> EFEE World Conference on Explosives and blasting in Helsinki 15<sup>th</sup> – 18<sup>th</sup> September 2019 are almost completed. Last week I took part in the menu tasting for the gala dinner and I can only reveal that our gala quests are up to a treat concerning all - food, wine and program.

Technical papers have been selected as well, I would like to thank our prestigious technical committee for all

the hard work. We received around 70 proposals for technical papers and the most interesting 45 were selected to be presented in the conference. The selection task was not easy due to unusually high quality of papers. I would like to take this opportunity already now to thank all who submitted their proposals and congratulate those who were selected. I am looking forward to listening into as many as possible of them.

The 2<sup>nd</sup> circular was published in early May and the registration has started. The early bird rate is valid until end of July. Please visit [efee2019.com](http://efee2019.com) in order to view the list of accepted papers, take benefit of the early bird registration rate, book your spot at the workshop, gala dinner and the post-conference excursion to a working dynamite factory. They are all expected to sell out early due to limited number of seats available.

All 60 exhibition booths will most likely also sell out as well but there are a couple of exhibition booths still available as I am writing this. Please book your booth quickly to be able to display your products and services to our international and professional delegates.

I wish you will enjoy reading this Newsletter and that you will have a nice summer and enough time to enjoy it also without hard hats and away from all the interesting blasting business. Personally I am looking forward to spending much time on the golf course and on the boat cruising the clean waters of the Finnish archipelago – there is nothing better and more beautiful in life.

After the summer I am looking forward to meeting many of you in my beautiful and vibrant home town Helsinki 15-18 of September – you are all welcome to Finland!

Jari Honkanen, President of EFEE



## Christer Svensson in Memoriam

On May 2nd the Swedish inventor and entrepreneur Christer Svensson, founder and former Chairman of Sigicom, passed away with his family by his side, in Stockholm, Sweden at the age of 72.

In 1981 Christer Svensson, a true innovator at heart, founded Sigicom. In the early years, the small family business mainly developed and delivered innovative monitoring equipment for blasting and other applications.

Through the following four decades he developed increasingly sophisticated solutions to modernize remote monitoring and measuring of vibration, noise, dust and other environmental disturbances on building sites around the world. With a keen eye to sophisticated digital sensor, presentation and internet technologies, he masterminded the conceptual and hands-on development of the company's INFRA system.

After receiving a life-threatening diagnosis some years ago, Christer Svensson dedicated even more time and relentless energy to ensure continued technological and business development. On a practical note, he increasingly focused on customer insight and technology development, gradually handing over company management to the next generation. This extended transition period has effectively resulted in a smooth transition and a clear vision for the company's future.

Outside of Sigicom, Mr. Svensson has made numerous friends around the world, and was a major contributor of knowledge and experience to several relevant industry organizations and standardization committees.

Christer Svensson will be greatly missed. He will always be remembered as a true visionary, a humble, soft-spoken leader and entrepreneur, a good listener, and an insightful and creative problem solver. The entire Sigicom team is dedicated to bring this unique heritage into an even greater future.

*Sigicom is a corporate member in EFEE and the entire EFEE administration and community wishes to honor his great life achievements for the good of our industry and send our condolences to entire Sigicom community and Christer's family for their loss.*



*Crister Svensson*



# HELSINKI 2019

# INFRA

10th  
ANNIVERSARY

## 10th Anniversary World Conference on Explosives and Blasting Scandic Marina Congress Center, Helsinki | 15th - 18th September 2019

The 10th World Conference will be held in the superb city of Helsinki, Finland from Sunday 15th to Wednesday 18th September at the Scandic Marina Congress Center overlooking the waterfront and a short distance from Helsinki's beautiful city centre.

This unique event draws attention from explosives users, manufacturers and drilling equipment operators as well as researchers and professionals involved in the construction and mining industry.

### The conference programme includes

- Large industry exhibition including the biggest names in the sector
- Technical programme featuring:
  - Blast Design Management
  - Blast Vibration and Seismology
  - Blasting Work Experiences
  - Construction, Mining & Quarrying (Blasting)
  - Demolition Blasting
  - EU Directives & Harmonisation Work
  - Explosive Detection for Security
  - Health, Safety & Environment
  - New Applications and Training
  - Shot Hole Development
  - Technical Development
- Industry specific workshops and tours
- Spectacular Finnish Gala Dinner

Supported by



Early bird conference registration will be available from March to July 2019



For further details visit [www.efee2019.com](http://www.efee2019.com) or email [info@efee2019.com](mailto:info@efee2019.com)

## Blast design and analysis from aerial imagery

### ABSTRACT:

Remote-controlled camera drones have reached a level of maturity which allow their routine application in mining and quarry for acquiring aerial imagery at high quality and resolution. Further developments in computer vision science allows for the rapid and consistent processing of a large set of highly overlapping pictures to registered 3D images. With 3D images several surveying and assessment tasks in surface mining are addressed. The use of aerial imagery from drones increases these possibilities and allow for the determination of several parameters (key performance indicators) that are utilised to benchmark and audit the results of drill and blast works in mining in surface operations.

### 1. INTRODUCTION

Drones (so-called unmanned aerial vehicles) have experienced a rapid development and maturity and are applied today by a broader user base. Remote-controlled and GPS-tracked devices are frequently used not only by consumers but also surveyors and related professionals. In particular the attachment of cameras to drones (fixed or with gimbal) enhances their use for 3D imaging technology from aerial imagery. Nowadays, 3D imaging from drones has found its way to surveying tasks in surface mining and quarrying.

3D images have been used in the past for specific task related to surface mining and quarrying, mainly originating from terrestrial imagery. The tasks included 3D bench face profiling and designing of blasts, and also geometric rock mass characterisation. This article reviews and addresses the various possibilities utilising aerial 3D images in surface mining showcasing that a single data set is useful for several applications such as:

- Blast design and analysis
- Volumetric measurements
- Excavation planning
- Stability assessment
- Fragmentation analysis
- Updating mine maps
- General documentation purposes

In the following section a brief overview on 3D image generation is given as well as the application of 3D images for surface mining which is addressed by various examples.

### 2. 3D IMAGE GENERATION

Photogrammetric reconstruction of surfaces recover 3D information using at least two photos from different angles where the photos show the same part of a "scene", e.g. a rock surface. The technology behind is called photogrammetry and dates back to 1850 (cf. Slama 1980).

In the 1990's upcoming digital imaging and availability of computing power brought new algorithms and new applications to image based stereoscopic measurement and led to the introduction of the term Computer Vision (cf. Faugeras 1993). This technique has been used mainly in robotics but also for geometric rock mass characterisation (Gaich et al. 2003).

A more recent approach handles multiple photographs simultaneously in order to perform a fully automatic 3D reconstruction. This technique is known as Structure from Motion (Snavely et al. 2008). Structure from Motion has reached maturity in the Computer Vision domain but the number of applications using the technique remained rather low. Although the geometrical principles have been developed in the 1990's it took till the

2010's where an application to high resolution input photos has been realised mainly for the reconstruction of objects from unordered image collections obtained from Internet user photo galleries (Snavely et al. 2008). Photogrammetry and Structure from Motion have merged then which brought Structure from Motion also to measuring and surveying tasks (cf. Pollefeys et. al. 2001, Hoppe et al. 2012).

In parallel to the evolvement of photogrammetry the availability of small lightweight drones highly rose. The broad utilisation of drones increased the abilities of photogrammetry especially in surface mining. The better angle of the camera to the areas of interest overcame potential occlusions that often occurred in sole terrestrial imaging. Terrestrial imaging, however, is still beneficial for vertical walls and high image resolutions and might be nicely combined with aerial imagery.

An important requisite for comprehensive and accurate 3D models in this context is redundancy in form of having the same part of the surface visible in several images. This redundancy allows to close gaps that pure stereoscopic photogrammetry may deliver and it has the potential to increase the accuracy of single 3D surface points. It furthermore enables the determination of the camera distortions on the fly, i.e. it allows to calibrate the camera while doing the project (auto-calibration).

Applying the principles of the Structure from Motion, 3D images are processed immediately on site or off-site using a cloud based service. The first requires according computing power on site, the latter needs a transfer of potentially large amounts of data over a network in order to send the photos and receive the results. Several software packages exist that allow for a close-to-fully automatic processing of image data to consistent 3D models.

Figure 1 left shows a picture of a drone in a surface mine. It carries an off-the-shelf SLR camera and in this case flew the bench face and the muck pile before hauling. On the right side a stack of images is displayed, the overlap between the images was approx. 85%, i.e. each part of the surface is visible in at least 5 images.



Figure 1: Drone ready for take-off in a surface mine (left) and stack of highly overlapping images (right).

Figure 2 showcases a crucial step for reaching accurate results in multi-photo reconstruction – the determination of the camera locations based on identified correspondences between the photos. In the example the drone flew operator controlled hence the “grid” of camera locations is not regular.

Figure 3 presents a snapshot of a 3D image taken of deposited tunnel excavation material in order to document the heap and to measure its volume. The computation of the 3D image requires the user to define a region of interest for the 3D measurements (optional), all other computation steps perform automatically.

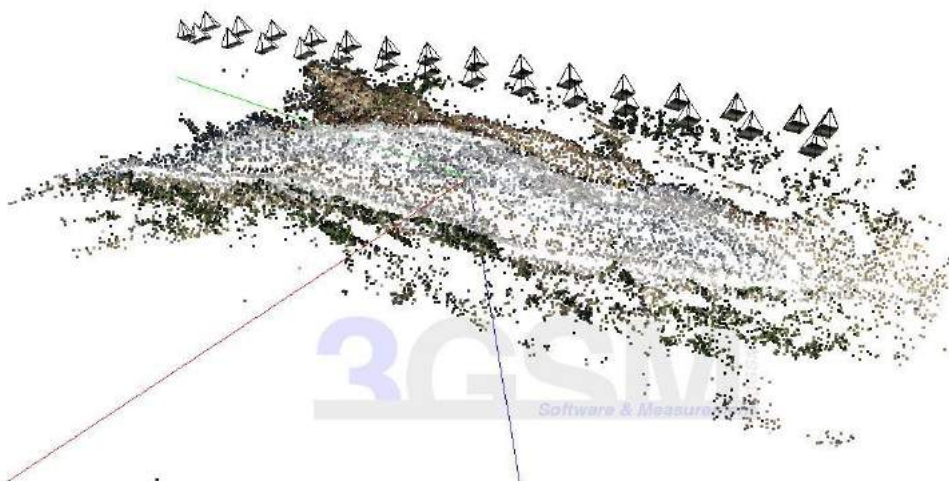


Figure 2: Intermediate result during 3D image generation: the small pyramids indicate recovered camera locations based on a subset of 3D surface points.

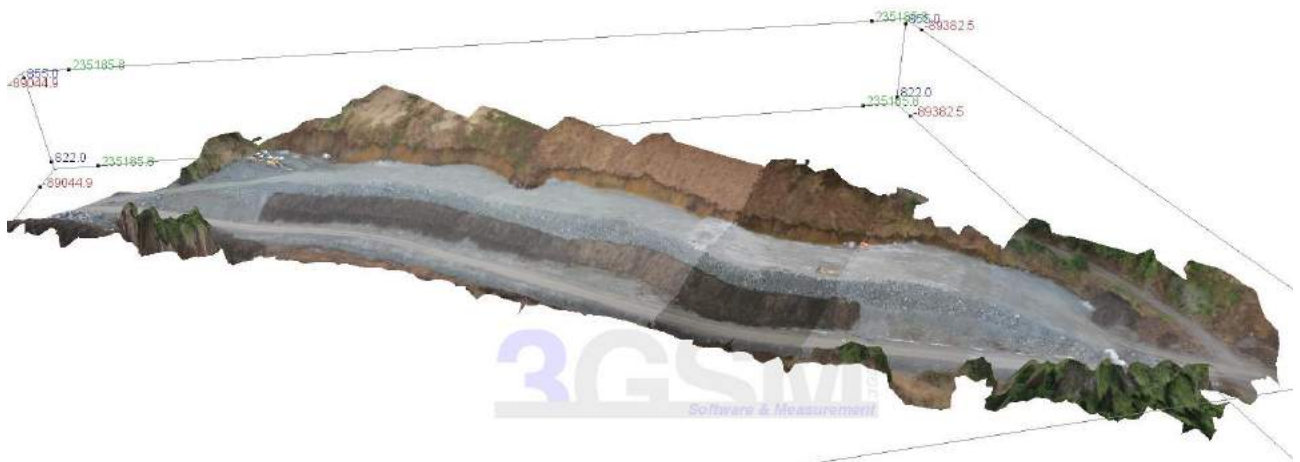


Figure 3: 3D image of a deposit (ca. 300 x 50 m)

### 3. THE APPLICATION OF 3D IMAGES IN SURFACE MINING

There are several reasons why aerial 3D imagery fits so well to surface mining sites: (i) large areas need to be acquired (surveyed), (ii) several parts are difficult to access or not accessible (e.g. highwalls), (iii) usually no vegetation obstructs the rock surface, (iv) drone flights over uninhabited areas are easier to perform from the legal point of view. The following sections showcase examples for 3D image generation from drone imagery applied in a surface mine and thus demonstrate its fields of application.

#### 3.1 Blast design

Incomprehensive knowledge on the geometry of a blast site and especially the face may lead to unexpected blasting results (Moser et al. 2007). Economic consequences of poor blasting in a surface mine or quarry include:

- ⌢ Additional efforts for loading and hauling
- ⌢ Efforts for secondary breakage
- ⌢ Too much fines
- ⌢ Reduced crusher performance
- ⌢ Additional wear of equipment due to uneven floors

More importantly, safety-related issues are also associated with:

- ⌢ Fly rock incidents
- ⌢ Excessive vibrations
- ⌢ Air blasts
- ⌢ Excessively damaged rock walls and floors leading to safety hazards

3D images provide a straightforward data basis for improving blasting results as they provide both (i) detailed information on the geometry of the blast site and (ii) a visually clear and detailed representation of the rock mass conditions. They enable to proactively design and optimise the drill pattern and loading according to the actual bench face geometry. This becomes a particular evidence at irregular bench faces, blasts with several free faces, or very large blast sites. The comprehensive data set from an aerial 3D image enhances the information of a face profile. It additionally provides the detailed geometry of the top of bench and in particular the conditions along the crest line.

Once the 3D image is generated and the drill pattern specified, real burden information is available, i.e. the distance from the borehole to the closest location of the free surface in any direction (360° spherical search). The 3D image may be coloured according to the current burden situation with reference to the design burden and a site-specific corridor of acceptance. Current burden values within the corridor of acceptance are coloured green while burden values below or above are coloured red or blue, respectively; hence making problematic areas obvious. By overlaying the colour codes to the 3D image, a self-explaining representation of the burden situation results (see figure 4).

In a proactive design approach, this information is used to adjust the location and/or the inclination of certain boreholes in order to adapt to the bench face geometry. Adjustment criteria may include minimisation of light and heavy burden areas or avoidance of (too) small borehole spacings.

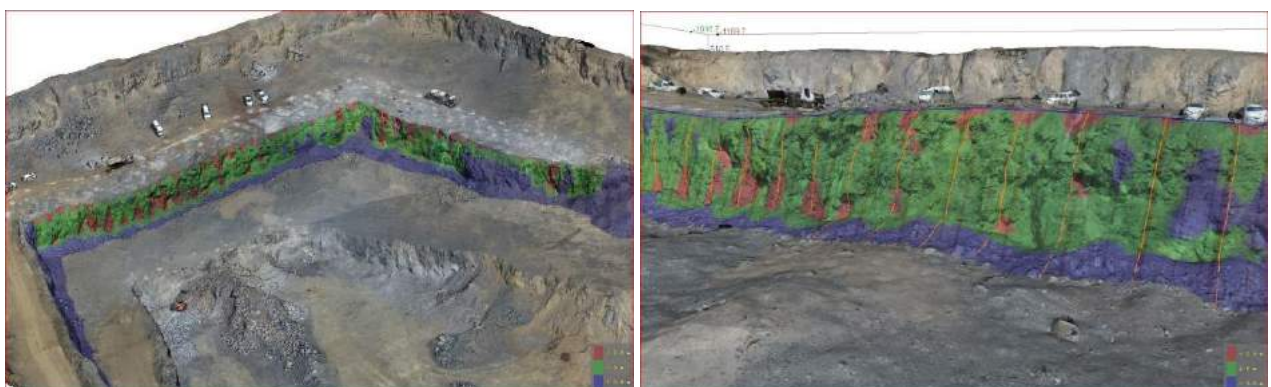


Figure 4: 3D image of a blast site including colour-coded visualisation of burden over the bench face area (left); detailed view with borehole profile locations (right). Green: design burden; Red: light burden; Blue: heavy burden

The so-called minimum burden is the key information for the optimisation of a drill pattern (cf. Moser et al. 2007). Since aerial 3D images provide detailed information on the top of bench, borehole length can be easily designed to match a horizontal plane or ramp. The result is a borehole map with co-ordinates for each borehole collar, the length, inclination, and bearing for each hole, as well as corresponding profile/burden data.

A complete blast design requires to audit the pattern as drilled, i.e. each borehole location and its course. Several sophisticated possibilities exist such as GPS with rover receiver, drill rigs with included GPS, down-the-hole probes, and drill rigs with such measurement possibility included. A basic method to audit as drilled borehole collars is the use of a tape measure along and across a predefined reference line. Aerial 3D images of blast sites with already drilled holes also allows to audit the collar positions directly (see left). In such cases neither a rover receiver nor GPS on the rig is required.

Figure 5 right shows the bank volume of the readily designed and audited blast. Together with the updated burden charts from the audit and the according profile plots, this provides information for an adequate loading of the holes.

(Stewart 2017) describes the geometric and economic impacts of proactive blast design including auditing using 3D images: Production time was reduced by 10% and the efforts for secondary breakage went down significantly.

The 3D image survey of section includes information before executing the blast (pre-blast survey). A drone flight after the blast allows for the analysis of the muck pile and its fragmentation (post-blast analysis). The post-blast 3D surface needs to be registered in the same co-ordinate system in order to enable comparative analyses. This is usually accomplished by geo-referenced surveys. If geo-referencing is not available, it is still possible to register the 3D models in a common local co-ordinate system based on common parts in the pre- and post-blast survey that remain unchanged in the 3D images.

Figure 6 depicts an overlay of two 3D images (pre- and post-blast) as well as a vertical section through the model. The resulting graphs visualise the shape of bench face and muck pile at this location. The power trough becomes obvious. Its location and depth is determinable simply from the data.

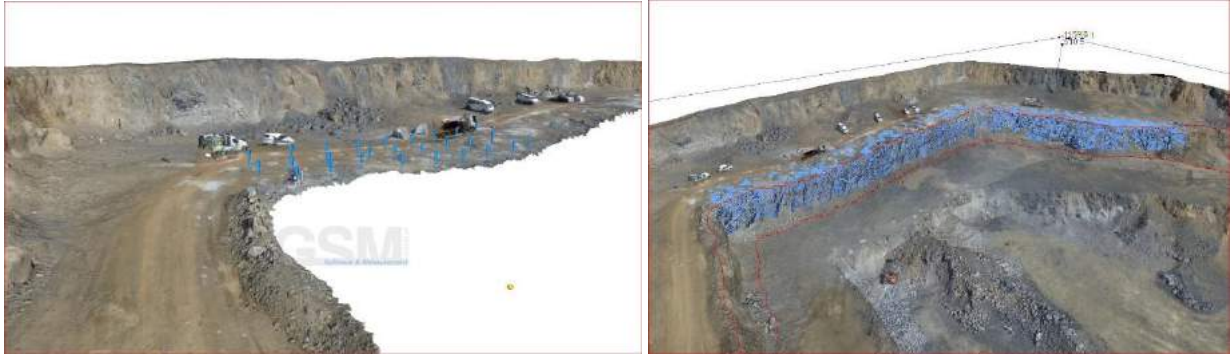


Figure 5: Blast site audit: the collars of the boreholes as drilled are visually determined from a 3D image – the collar locations are indicated by blue arrows (left); estimated pre-blast volume for the shot also indicated in blue (right).

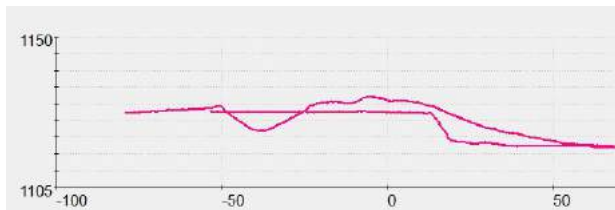
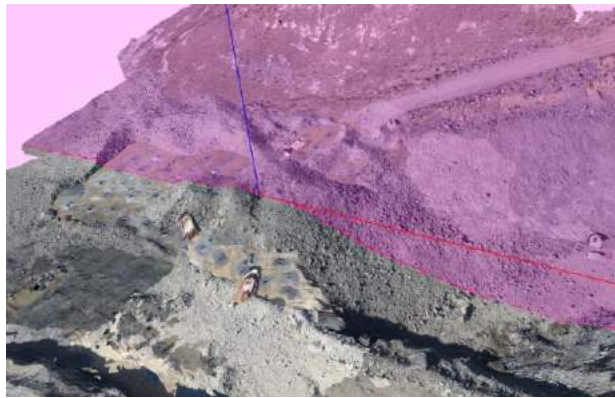


Figure 6: A section through 3D surfaces pre- and post-blast reveals the shape of the muck pile and allows the determination of depth and location of the power trough (arrow).

### 3.2 Post-blast analysis

The volume of the muck pile is determined by the comparison of the two surfaces pre- and post-blast. The embedded volume between the surfaces corresponds to the volume (see figure 7). Note that the precise volume of the muck pile is available once the whole muck pile has been cleared from the new free face. So, only a third drone flight after mucking (post-mucking survey) enables the precise determination of the blasted volume, the real bank volume, and the accurate volume of the muck pile. With this information at hand the swell as the ratio between the muck pile volume and bank volume is determined.



Figure 7: Volumetric description between two arbitrary shaped surfaces.

Another key parameter for describing blasting results is the distribution of particle sizes (fragmentation). Several software solutions are offered on the market. Some rely on the segmentation of particles by 2D image analysis (e.g.

Split, WipFrag). The required scale information is introduced either by objects of known size in the photos or by basic stereoscopy with known camera distances (Motion Metrics). Also geometric approaches exist (Thurley et al. 2015) performing an analysis of the shape of the muck pile. Using 3D images, both ideas nicely combine and enable taking out the best of both

approaches. shows a section of a 3D image from a muck pile and the resulting delineation of particles. The applied algorithm analyses the shape of the surface and combines the result with image processing algorithms.

3D images form a self-explaining type of documentation. Whenever an incident occurs, the presence of data that is easily communicated also to non-experts in the field is beneficial. In addition to the 3D images the generation of a video document of the blast is useful. The video additionally enhances the means of communication as mentioned.

Topographic maps are inherently generated from 3D images and are available for free when performing blast design or blast documentation. Figure 9 shows a topographic map from a part of a surface mine where a blast site has been designed.

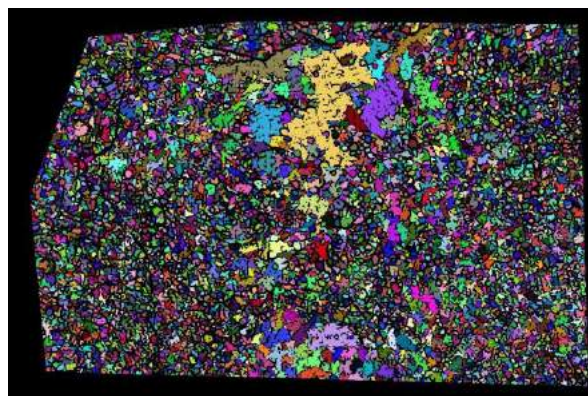


Figure 8: 3D image of a muck pile (left) and automatic particle detection based on the combination of geometric analysis and image processing (right).

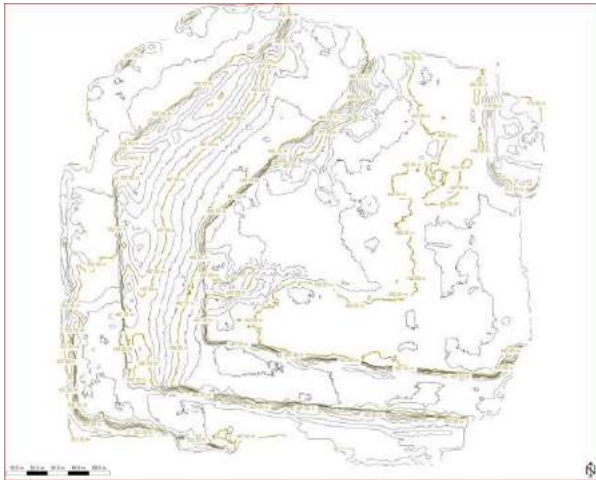


Figure 9: Topographic map of a surface blast site and its adjacent benches and ramps.

### 3.4 Geometric rock mass characterisation

The natural representation of the rock surface with a 3D image allow for qualitative and quantitative assessments. Qualitative assessments include the face quality in general and the presence of open and/or large joints, cavities, or weak zones, e.g. mud seams or faults.

For a quantification of (geometric) rock mass properties spatial measurements are required. Software tools exist that enable the determination of joint orientations, joint sets and their spatial variation, as well as quality parameters such as joint frequency, or joint spacing. Such characterisation of the rock mass may also happen automatically or semi-automatically. Approaches as described by (Slob 2010, Riquelme et al. 2014) aim to identify planar regions in 3D point clouds.

Figure 10 and figure 11 outline the principle of a topographic analysis of a 3D surface. The basis is the set of normal vectors over the surface. Their spatial distribution resp. their density lead to clusters of the normal vector's orientation. The clusters are then used in a second processing step for the generation of areas that may correspond with joint surfaces (see figure 11).

The possibilities within quantified rock mass characterisation provide a profound data basis for defining the geometric parameters of a fractured rock mass such as the number of joint sets, joint set orientations and its variation, joint set spacing and its variation, joint set persistence, etc. High resolution surveys also enable the measurement of the waviness and roughness of the exposed joint surfaces. The basic input parameters for stability assessments of benches, inter-ramp slopes and overall pit slopes are quickly available, and can be easily audited additionally.

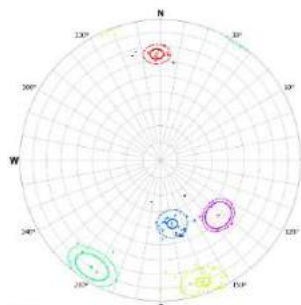
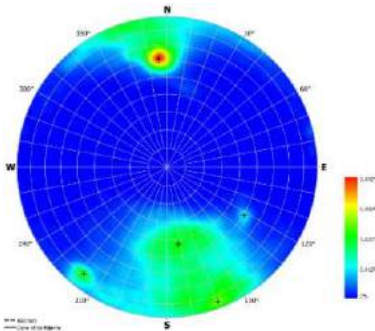
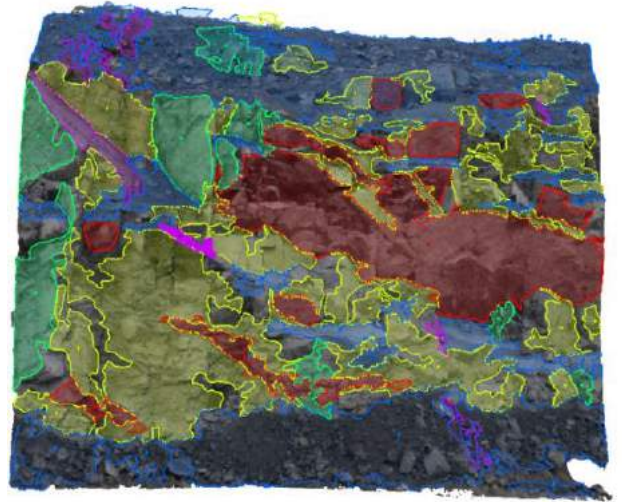


Figure 10: Section of a bench face (left) and automatically analysed orientations of surface normal including colour-coded density distribution (right)

Figure 11: Automatically determined surface areas, clustered according to their spatial orientations (left) and according plot in the stereo net (right).

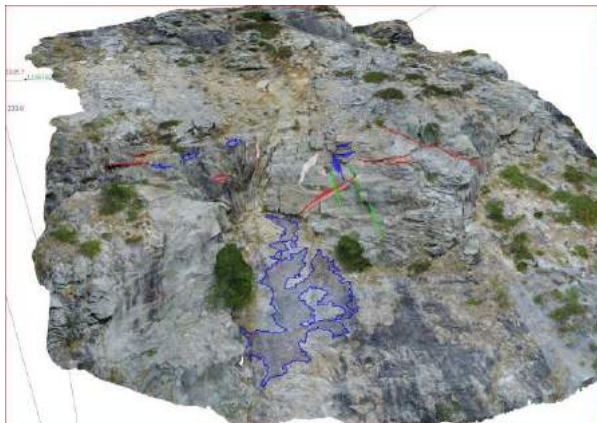


Figure 12: Basic geologic mapping of a rock wall area with difficult access forms the basis for stability assessments.

#### 4. CONCLUSIONS

The use of aerial 3D imagery taken with drones allows for performing several surveying and assessment tasks in surface mining and allow for the determination of several key performance indicators. The consequent determination of such parameters lead to comparable results between different blasts and shall help to improve the quality of drilling and blasting works in terms of productivity and efficiency while still preserving high safety standards. Surveying and assessment tasks related with the application of aerial 3D images include:

- Ĥ Surveying of bench face, top, and floor
- Ĥ Face profiling – pattern, profiles, minimum burden
- Ĥ Blast design
- Ĥ Post-blast analysis
- Ĥ Rock mass characterisation - geological mapping
- Ĥ Mine plan update
- Ĥ General documentation

Key performance indicators determined from 3D images:

First drone flight (pre-blast):

- Ĥ Pre-blast volume – as designed (prediction)
- Ĥ Pre-blast volume – as drilled (prediction)
- Ĥ Location of hole collars
- Ĥ Thickness of seams, orientation, location (geological mapping)

Second drone flights (post-blast before mucking):

- Ĥ Volume of the muck pile (estimation)
- Ĥ Bank volume (estimated)
- Ĥ Height and width of the muck pile
- Ĥ Power trough volume
- Ĥ Power trough cross sections – location of minimum
- Ĥ Fragmentation distribution
- Ĥ Visible half barrels – Number, average length, total length

Third drone flights (after mucking):

- Ĥ Volume of the muck pile (real)
- Ĥ Bank volume (real)
- Ĥ Percent cast as a volume ratio
- Ĥ Swell of the muck pile volume
- Ĥ Back break – Distances, Volumes
- Ĥ Number and length of half barrels and burn cuts

Using aerial 3D imagery from drones covers a wide range of application in surface mining making this technology a viable standard operating procedure.

## 5. ACKNOWLEDGEMENTS

Part of the work was funded from the European Union's Horizon 2020 research and innovation programme under grant agreement No. 730294.

## REFERENCES

- Faugeras, O. 1993. *Three-Dimensional Computer Vision*. MIT Press, Boston, MA.
- Gaich, A. Fasching, A., Schubert, W. 2003. Improved site investigation. Acquisition of geotechnical rock mass parameters based on 3D computer vision. In G. Beer (ed.) *Numerical Simulation in Tunnelling*, Springer, Wien New York, pp. 13-46.
- Hartley, R. & Zisserman, A. 2001. *Multiple View Geometry in Computer Vision*, Cambridge University Press, UK.
- Hoppe, C., Klopschitz, M., Rumpler, M, Wendel, A., Kluckner, S., Bischof, H. & Reitmayr, G. 2012. Online feedback for structure-from-motion image acquisition. In *British Machine Vision Conference (BMVC)*.
- Moser, P., Ganster, M., Gaich, A. 2007. Experience with and benefits from the use of 3D Stereophotogrammetry for blast design and control, *In Proc. of the 33<sup>rd</sup> annual conference on explosives and blasting technique, Nashville, TN, Vol. I:* 315-327.
- Motion Metrics International Corp. <http://www.motionmetrics.com/portable/>
- Pollefeys, M., Van Gool, L, Vergauwen, M., Cornelis, K., Verbiest, F., & Tops, J. 2001. Image-based 3d acquisition of archaeological heritage and applications. In *Proceedings of the 2001 Conference on Virtual Reality, Archeology, and Cultural Heritage*, pp. 255-262.
- Riquelme, A. J., Abellán, A., Tomás, R., & Jaboyedoff, M. 2014. *A new approach for semi-automatic rock mass joints recognition from 3D point clouds*. *Computers & Geosciences*, 68, 38-52.
- Slama, Ch. C. (ed.) 1980. *Manual of Photogrammetry*. 4th edition. American Society of Photogrammetry, Falls Church, VA.
- Slob, S. 2010. *Automated rock mass characterisation using 3-D terrestrial laser scanning*. PhD thesis, TU Delft, ISBN 978-90-9025364-0
- Snavely, N, Seitz, S.M. & Szeliski, R. 2008. Modeling the World from Internet Photo Collections. *International Journal of Computer Vision*: 80(2):189-210.
- Split Engineering LLC. <http://www.spliteng.com>
- Sterwart, D. 2017. Drill and Blast Improvement Project Using Photogrammetry, GPS and Drill Navigation Systems. In: *Proceedings of 43rd Annual Conference on Explosives and Blasting Technique*, Orlando, FL.
- Thurley, M.J., Wimmer, M. & Nordqvist, A. 2015. *Blast measurement based on 3D imaging in sublevel caving drawpoints and underground excavator buckets at LKAB Kiruna*. *Fragblast 11*, pp. 1-17. Sydney.
- Triggs, B., McLauchlan, P.F., Hartley, R.I, & Fitzgibbon, A.W. 2000. Bundle adjustment - a modern synthesis. In *Proceedings of the International Workshop on Vision Algorithms: Theory and Practice*, pp. 298-372.
- WipWare Inc. <http://www.wipware.com>



## Solution-oriented blasting services



We manufacture and deliver explosives and provide blasting related services for our customers. Our comprehensive product repertory consists of Bulk emulsion and cartridge explosives as well as other blasting accessories.



Read more about our services on >> [FORCITGROUP.COM](http://FORCITGROUP.COM)



50 years of expertise | 100 professionals | 2000 measuring instruments

# Strongest in the Nordics by any measure

Leading provider of blasting and vibration consulting in Northern Europe.



Norway and Sweden



Sweden



Finland



NEWSLETTER July 2019  
[www.efee.eu](http://www.efee.eu) /[newsletter@efee.eu](mailto:newsletter@efee.eu)

BACK TO TOP

## Testing of a full- scale building under external blast

**ABSTRACT:** Building structures should have sufficient robustness to resist progressive collapse that can result from localized failures (e.g. due to blast). However, current codes governing the design for robustness are rather generic and have limited provisions ensuring that structures withstand the exposure to such threat. Due to the complexity of the phenomenon (blast pressure, dynamic response, level of damage, residual capacity, propagation of collapse), the experimental validation of full-scale models may still be necessary for the development of numerical or analytical tools. An ongoing national research project, aiming to develop and validate numerical models for predicting the blast response of a steel framed building is under development. The building will be subjected to blasts (TNT or equivalent) with different charge sizes and locations, resulting in different scaled distances. As the scaled distance reduces, the peak overpressure increases, thus causing the shear failure of the elements located in the proximity. The potential for progressive collapse following local damage will be also investigated.

different combinations of charge weights, standoff distances and levels of gravity load on the building floors. The preliminary validation of the numerical model is done using the results of blast tests, which were performed on similar steel frames within a previous research project.

### 1. INTRODUCTION

In urban areas, blast events have a low probability of occurrence but pose significant risks for civil facilities (significant damages, collapse) and people (injuries, fatalities). Such attacks have recently emerged at the global scale due to terrorist actions and regional conflicts. Because the blast hazard cannot be eliminated, risks can be reduced by diminishing the exposure and/or vulnerability of people and assets. Blast pressure is typically substantially greater than other loads considered in structural design, but it decays exponentially with distance and time. Providing an adequate standoff will therefore substantially reduce the exposure by decreasing the maximum pressure. Enhancing the local strength of building components to resist failure and creating alternate load paths are means to reduce the vulnerability and prevent the progressive collapse of buildings, which is the cause of injuries and fatalities. The ability of a structure to withstand extreme loading events without being damaged to an extent disproportionate to the original cause is called structural robustness (EN 1991-1-7). Awareness of risk requires appropriate measures in the design and construction of buildings (ASCE, 2011; DoD, 2014). Due to the complexity of the phenomenon (blast pressure prediction, dynamic response, damage level, structural residual capacity), more accuracy can be obtained if results are checked against data from tests on similar structures. Reviews of the international research on structural robustness and disproportionate collapse (CPNI, 2011; El-Tawil et al., 2014) highlighted this need for detailed

testing data and improved modelling and design guidance. Some contributions to the development of robustness provisions have been obtained within European projects COST TU0601 (2007-2011), COST C26 (2006-2010), ADBLAST (2010-2013), CODEC (2012-2016). Magallanes et al. (2006), F. Fu (2013), Ralston et al. (2015), Kernicky et al. (2015), Zhang et al. (2016) also investigated the behaviour of structures under blast loads. The difficulties and risk in developing real blast tests transferred most of the research to column loss tests (or similar) under static or dynamic conditions (Astaneh-Asl et al., 2001; Sadek et al., 2008; Alashker et al., 2010; Demonceau & Jaspert, 2010; Xu & Ellingwood, 2011; Yang & Tan, 2013; Song et al., 2014; Mazurkiewicz et al., 2015; Dinu et al., 2015, 2016.a,b,c).

As seen, the issue of structural robustness under blast loading is of high interest worldwide, and is on the agenda of many public and private institutions. In this regard, the study deals with the preliminary analysis of a full-scale building model against blast. The study is part of a research project (FRAMEBLAST, 2017-2018), which aims at providing the validation of the response of a full scale building structural frame system under blast loading conditions in laboratory environment. The building will be subjected to blasts (TNT or equivalent) with different charge sizes and locations. As distance reduces, the peak overpressure increases, causing the shear failure of the elements located in the proximity (Dinu et al., 2016.d). After the loss of one column, the redistribution of loads and development of alternate load paths (through flexural, arching, and catenary behaviour) will be mobilized and the performance of connections will be validated.

Preliminary blast tests on 3D frames were performed for the primary calibration of the numerical model in Extreme Loading for Structures ELS. Frame specimens, like those of the full-scale building structural frame, were tested inside a bunker using different blast charges.

## 2. CONFIGURATION AND DESIGN OF THE FULL-SCALE BUILDING MODEL

The full-scale building model is a two-span, two-bay, and two-story steel structure ( .a). The bays and spans measure 5.0 m and 3.0 m, respectively, while each story is 2.5 m high, see .b-c. The structural system is made of moment resisting frames on the transversal direction, while on the longitudinal direction it is made of concentrically braced frames placed on perimeter frames. The extended end-plate bolted beam-to-column connections in the moment resisting frames are designed as fully rigid and fully restrained connections, see .d-e. Secondary beam-to-column connections and secondary beam-to-main beam connections are pinned connections, see .e-f. Columns are rigid at the base. The design of the structure for permanent and seismic (low seismicity, 0.10 g horizontal acceleration) design conditions resulted in an IPE 300 section for main beams and IPE 200 for secondary beams, while columns were HEB 260. Note that structural steel S275 (yield strength of 275 N/mm<sup>2</sup>) was used for beams and columns.

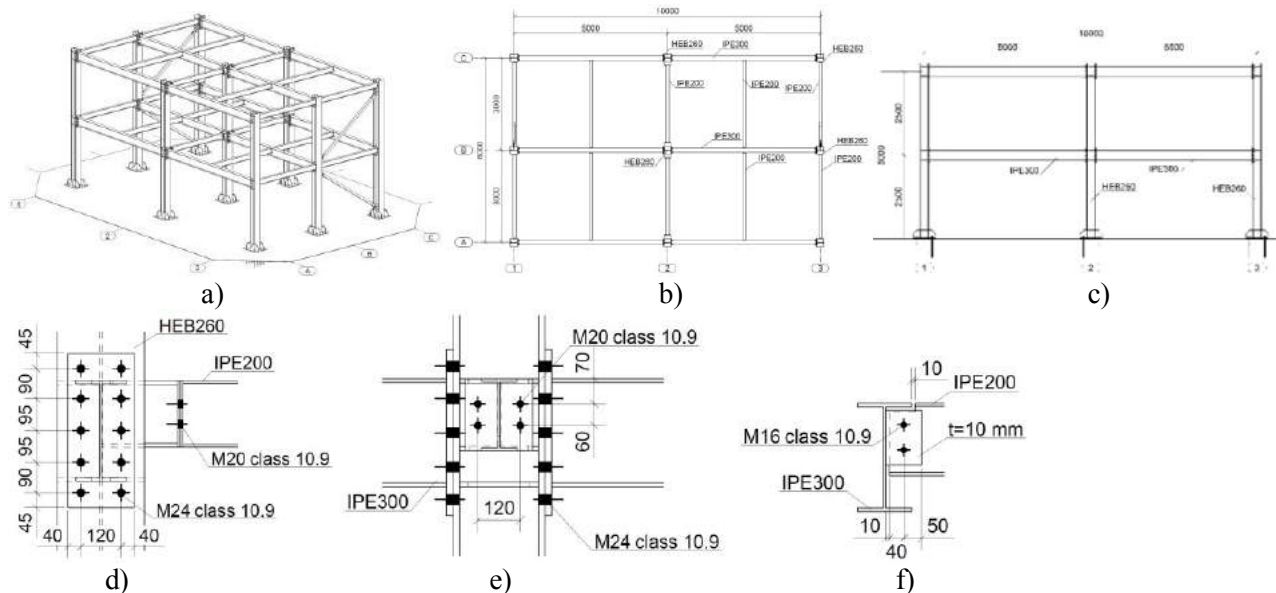


Figure 1. Views and details of the full-scale building model: a) 3D view; b) floor plan; c) transversal frame; d) beam-to-column connection; e) secondary beam-to-column connection f) secondary beam-to-main beam connection

As planned, the steel frame building will be subjected to high explosive charges detonated in the proximity of a column, see . Blast loading effects may produce specific local and global responses, each associated with a different failure mode. Local response is mainly characterized by direct shear or punching shear, and generally results from close detonations, while global response is typically manifested as flexural failure, and results from blasts at larger standoff distances. Therefore, for predicting the blast pressure and response of the structure in different loading scenarios, a parametric study has been developed.

First, in order to assess the progressive collapse resistance, blast charge is increased until a column is lost. Then, the level of gravity loads on the floors is incremented until the progressive collapse is initiated. The influence of the standoff distance is also assessed by comparing the effects of blast loadings with different charge weights detonated at different distances from the structure. The calibration of the numerical model is done using the results of blast tests performed on similar steel frames.

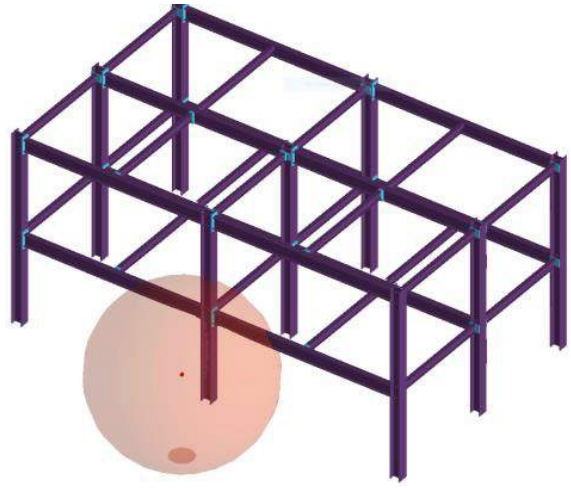


Figure 2. View of the structure with the position of the blast charge for external blast tests

### 3. PRELIMINARY CALIBRATION OF THE NUMERICAL MODEL

In order to have a close estimation of the effects of different charges on the structure (state of damage), preliminary nonlinear simulations were done using the Extreme Loading for Structures (ELS) software. Calibration of the model was done using tests performed inside a bunker on similar 3D frames. Two identical 3D specimens were designed and constructed for blast testing inside a bunker (Figure 3). Specimens were extracted from a typical moment resisting steel frame structure.

Specimens include a column (with the weak axis oriented in the plane of the frame), two half-span longitudinal beams rigidly connected to the column using extended end plate bolted connections, and one half-span transversal beam, connected to the column web using a simple clip angle connection. Lateral restraints made from tubular profiles were used at the ends of longitudinal beams. An IPE 220 section was used for beams, while columns were made from HEB 260, but with flanges reduced to a 160 mm width. The design steel material in plates and profiles was S275 J0 and bolts were grade 10.9. summarizes the measured material properties of the specimens.

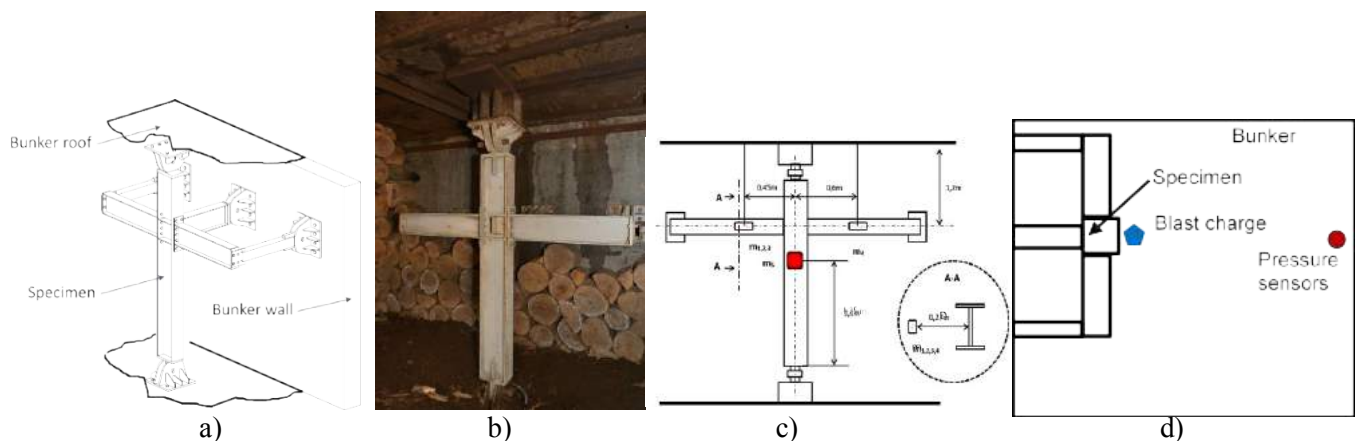


Figure 3. Test specimens inside the bunker: a) view of the specimen; b) photo inside the bunker; c) front view with the position of blast charges; d) plan view with specimen and pressure sensors inside the bunker

Table 1. Average characteristic values for materials in steel profiles, plates and bolts

Element	$f_y$ (N/mm <sup>2</sup> ) yield strength	$f_u$ (N/mm <sup>2</sup> ) ultimate strength	$A_{gt}$ (%) Total elongation at maximum stress
Beam flange IPE220, $t = 9.2$ mm	345	464	28.0
Beam web IPE220, $t = 5.9$ mm	353	463	30.4
Column web HEB 260, $t = 10$ mm	407	539	27.0
Column flange HEB 260, $t = 17.5$ mm	420	529	27.0
End plate, $t = 16$ mm	305	417	17.1
Bolt, M16 class 10.9	965*	1080	12.0

Note: \* 0.2% offset yield point

The main hazard components of an explosion are blast (overpressure), fragmentation, and thermal effect. In our study, only the first issue is of interest. The peak pressure value depends very much on the distance of the detonation point from the structure of interest. The effect of distance on the characteristics of blast can be taken into account by introducing the scaling laws (DoD, 2014). These laws have the ability to scale parameters, which were defined through experiments, in order to be used for varying values of distance and charge energy release (Karlos & Solomos, 2013). The most common blast scaling law is the one introduced by Hopkinson (1915) and Cranz (1923). According to the Hopkinson-Cranz law, a dimensional scaled distance is introduced as described by Eq. (1):

$$Z = \frac{R}{W^{1/3}} \quad (1)$$

where:

$Z$  is the scaled distance, in  $m/kg^{1/3}$ ,  $R$  is the distance from the detonation source to the point of interest [m] and  $W$  is the weight of the explosive [kg TNT or equivalent TNT].

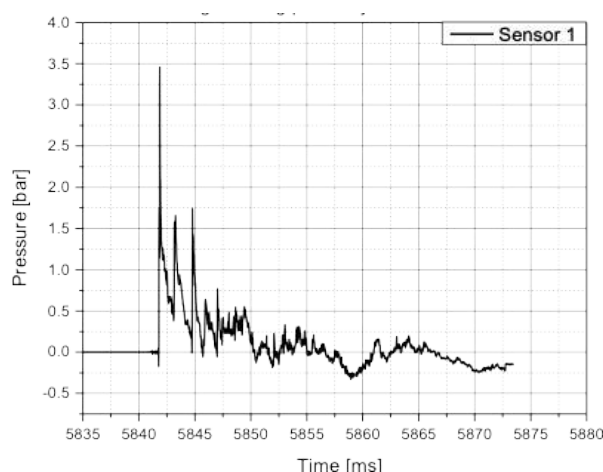
The calculation of the peak pressure of the shock wave generated by TNT-equivalent charge is made considering that pressure is a function that depends on distance, explosive charge and local conditions, being widely used the empirical formula proposed by Richards and Moore (2005) (Eq. (2)):

$$P = A \times \left( \frac{R}{(W)^b} \right)^a \quad (2)$$

where:

$P$  is the peak overpressure (in bar),  $A$  is the site constant (evaluated experimentally),  $a$  is the site exponent (evaluated experimentally, always negative),  $b$  is the site exponent for the charge weight (evaluated experimentally),  $R$  and  $W$  defined above.

Using experimental calibration tests, Eq. (2) can be used in case of bunker tests. In the study, calibration blast tests were performed first, in order to evaluate the site exponents  $A$ ,  $b$  and  $a$ . Then, the specimens were subjected to blast of increasing intensities, obtained by increasing the charge weight and/or reducing the distance from the blast to the specimen. In total, there were four blast charges with the following weights:  $m_1 = 121$  g,  $m_2 = 484$  g,  $m_3 = 968$  g, and  $m_4 = 1815$  g, all placed at distance  $D = 0.50$  m from the column web (see Figure 3.c) and one charge  $m_5 = 1815$  g, at  $0.50$  m from the column web (see Figure 3.c) and one charge  $m_5 = 1815$  g, at  $0.20$  m distance from the column web. The charges were freely suspended from the bunker ceiling. All charges were placed at a height of  $1.15$  m from the column base and  $0.25$  m from the bottom flange of the beam. In order to evaluate the site exponents  $A$ ,  $b$  and  $a$ , and then the pressure inside the bunker, two Kiestler pressure sensors were mounted on a special frame, at  $3.5$  m from the specimen, in front of the bunker venting (see Figure 3.d). The explosive material used in the testing has a TNT equivalence of 1. Note that the effects of gravity loads on the columns and beams were not considered in the test.



The pressure measurements done after the first four explosions were  $p_{1,max} = 0.31$  bar,  $p_{2,max} = 0.75$  bar,  $p_{3,max} = 1.22$  bar, and  $p_{4,max} = 2.23$  bar. The peak pressure during last explosion attained the maximum value,  $p_{5,max} = 3.5$  bar ( .a). With the values of the pressure measured during each detonation, the following specific coefficients of the bunker were determined:  $A = 3850$ ,  $a = -2.64$ ,  $b = 3.5$  bar (Figure 4.a).

With the values of the pressure measured during each detonation, the following specific coefficients of the bunker were determined:  $A = 3850$ ,  $a = -2.64$ ,  $b = 0.3125$ .

The peak pressure value of the blast wave decreased rapidly, along with the distance between the blast source and the target surface, as seen in Figure 4.b.

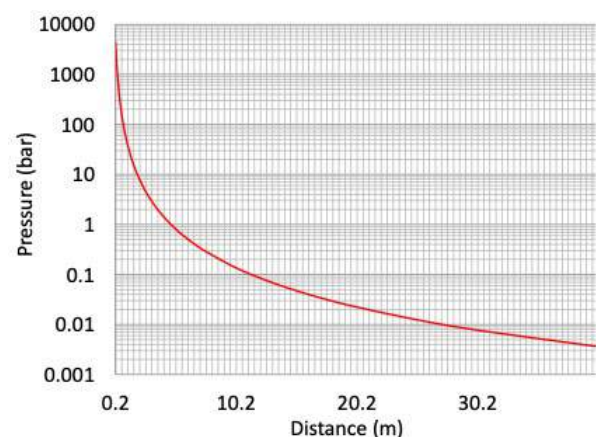


Figure 4. Pressure measurements for test with  $m = 1815$  g,  $D = 0.20$  m: a) pressure vs. time record; b) peak pressure vs. distance between the blast source and the target surface



a)



b)

Figure 5. Column web fracture,  $D = 0.20$  m,  $W = 1815$  g: a) specimen 1; b) specimen 2

For the first three explosions, there were no visible deformations at the level of the specimen, indicating the column is in the elastic range. However, for  $m_4$ , the results were different, i.e. for the first specimen the column web has been deformed plastically out of plane for approximately 22 mm, but without any visible cracks, while for the second specimen the deformations were 3 mm only. The differences could be attributed to the orientation of the blast charge at the time of detonation. The last charge,  $m_5$ , caused severe local deformations of the column for both specimens, with the web completely removed from the column. Longitudinally, the fracture line was located close to the fillet zone. For the first specimen, the web rupture extended for a length of almost 600 mm, while for the second specimen the rupture extended for 500 mm (Figure 5). The performance of the steel specimens undergoing close detonations was also predicted using ELS (2017). ELS utilizes a nonlinear solver based on the applied element method (Tagel-Din, H. & Meguro, K., 2000) which is a derivative of the finite element method and the discrete element method.

In ELS, the structure is modelled as an assembly of small elements, which are assumed to be connected by one normal and two shear springs located at contact points distributed around the element edges. The average normal strain is calculated by taking the average of the absolute values of strains on each face. When the average strain value at the element face reaches the separation strain, all springs at this face are removed and elements are not connected any more (until they collide). Columns, beams, and plates were modelled as solid elements and could undergo deformations at the interface between the discretized elements (Figure 6.a). The constraints, made of tubular sections, were also modelled as solid elements. The bolts were modelled using individual springs: one for normal stresses and two for shear stresses. The column bases and transversal beam end connection to the bunker wall were considered as pinned, and all displacements were prevented. Blast pressure was modelled using pressure impulse calculations as provided in UFC3-340-02 (2014). The reflected pressure was not considered in these numerical tests.

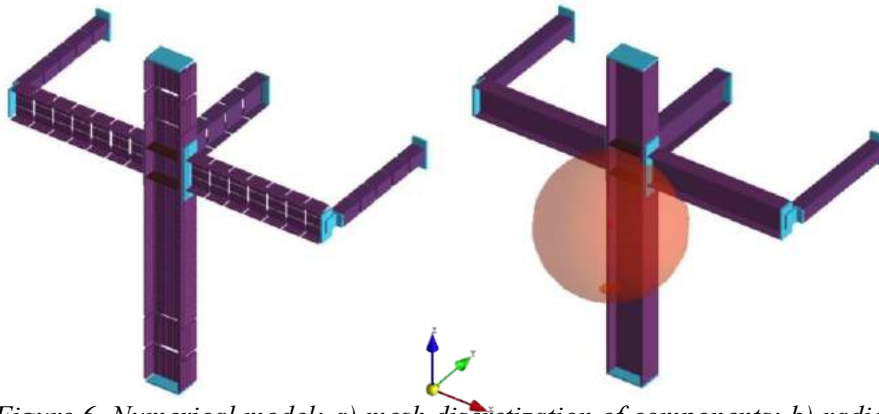


Figure 6. Numerical model: a) mesh discretization of components; b) radially expanding shock wave

Due to the dynamic (impulsive) character of the blast load, the effects of strain rates on the material are very important. The rate dependency has been considered by means of the following relationships (Kaneko, 1997):

$$\frac{f_{ysr}}{f_y} = 1 + \frac{21}{f_y} \log \frac{\dot{\epsilon}}{\epsilon_0} \quad (3)$$

$$\frac{f_{usr}}{f_u} = 1 + \frac{7.4}{f_u} \log \frac{\dot{\epsilon}}{\epsilon_0} \quad (4)$$

where:  $\dot{\epsilon}$  = strain rate,  $\epsilon_0 = 10^{-4}$   
 $f_y, f_u$  = yield and tensile strength in quasi-static conditions,  $\epsilon_0 = 10^{-4}$   
 $f_{ysr}, f_{usr}$  = yield and tensile strength at strain rate  $\dot{\epsilon}$ .

Because the strain rate is not initially known, an initial analysis is performed using static material properties, see Table 1. The strain rate is then calculated in the location of interest and material properties are corrected using Eq. (3) and Eq. (4). Figure 7 shows the fracture mode and deformed shape of the specimens and the displacement history (out of the web plane). The permanent deflection of the columns is very close to the measurements made after the test. Also, the extension of damage in the columns is very similar, with the same location and extension as for fracture lines.

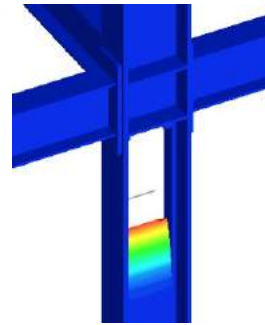


Figure 7. Fracture mode in the numerical simulation, ELS

#### 4. PARAMETRIC STUDY

The numerical model calibrated against test data was used to study the behaviour of the full-scale building model subjected to external blast loading. In the study, the parameters are the level of gravity load on the floors,  $G$ , the standoff distance from the building,  $R$ , and the charge weight,  $W$ . As seen from the experimental tests, a charge weight  $W = 1815$  g at a distance  $D = 0.20$  m causes a complete fracture of the column web. However, in the absence of any gravity loads, it is not possible to see if the severe damage in the column initiates the progressive collapse of the structure. The level of gravity loads is therefore a key parameter for the present study and is considered by means of a gravity load amplifier,  $\lambda$ .

The gravity loads for the entire structure are calculated using the following load combination:

$$G_{ND} = 1.2 DL + 0.5 LL \quad (4)$$

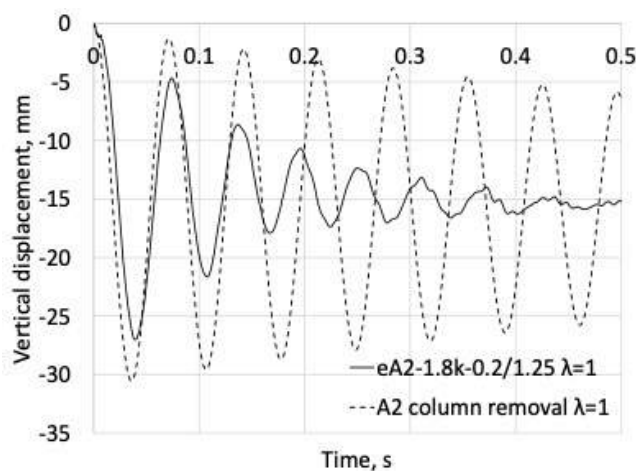
where:

$G_{ND}$  = Gravity loads for the nonlinear dynamic analysis; DL = Dead load (in kN/m<sup>2</sup>); LL = Live load (in kN/m<sup>2</sup>)

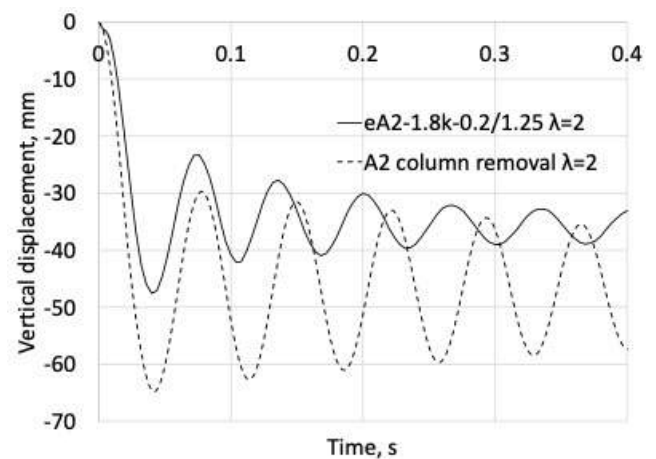
Dead load and live load are both considered as 4 kN/m<sup>2</sup>. The loading procedure starts from a zero load.

Then, gravity loads are monotonically and proportionately increased until equilibrium is reached. After the equilibrium is reached for the frame structure, the blast load is applied. The results are also compared with the notional removal of the column, which is the method used in the Alternate Load Path method (DoD, 2016).

Notations are as follows: eA2: location of the column affected by explosion; 1.8k: weight of the blast charge, in kg of TNT, rounded down to one decimal; 0.2/1.25: 0.2- distance to the column centreline (in meters) & 1.25 -height above the ground at which the blast occurs (in meters).



a)



b)

Figure 8 shows the history of vertical displacement for blast scenario eA2-1.8k-0.2/1.25, at three gravity load levels,  $\lambda=1$ ,  $\lambda=2$ , and  $\lambda=4$ . For the same gravity load levels, results are also compared with the notional column removal. Figure 9 shows the level of damage in columns and the deformed shapes also for blast scenario eA2-1.8k-0.2/1.25. As it can be seen, for the design level of gravity loads ( $\lambda=1$ ), the blast load causes severe damages in the column (Figure 9.a), but the progression of collapse is prevented (Figure 9.b). The flanges (that remained intact after the blast) cause a reduction in the dynamic amplification and the displacements are slightly lower compared to the notional column removal (Figure 8.a). For the maximum load amplifier,  $\lambda=4$ , displacements are very large, but the structure still resists the progressive collapse (Figure 8.b, Figure 9.c-d). Load amplifiers beyond this value will trigger the progressive collapse of the structure. This prediction is important because it will allow the determination of the amount of explosive and the gravity loads that are sufficient to eliminate a column and to cause large deflections in the structure, but without the progressive collapse of the entire (or large part) of the structure.

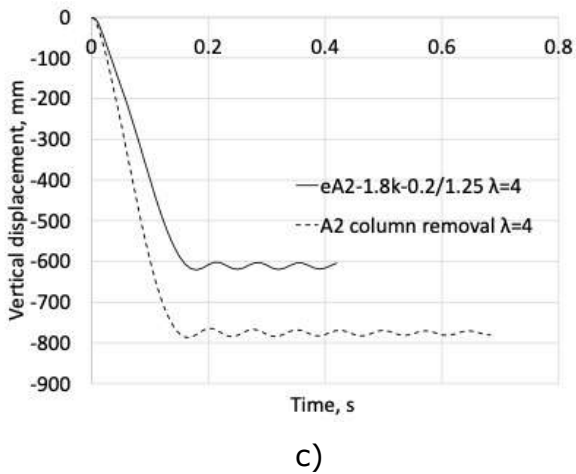


Figure 8. History of vertical displacement for eA2-1.8k-0.2/1.25 and notional column removal scenarios: a)  $\lambda=1$ ; b)  $\lambda=2$ ; c)  $\lambda=4$ .

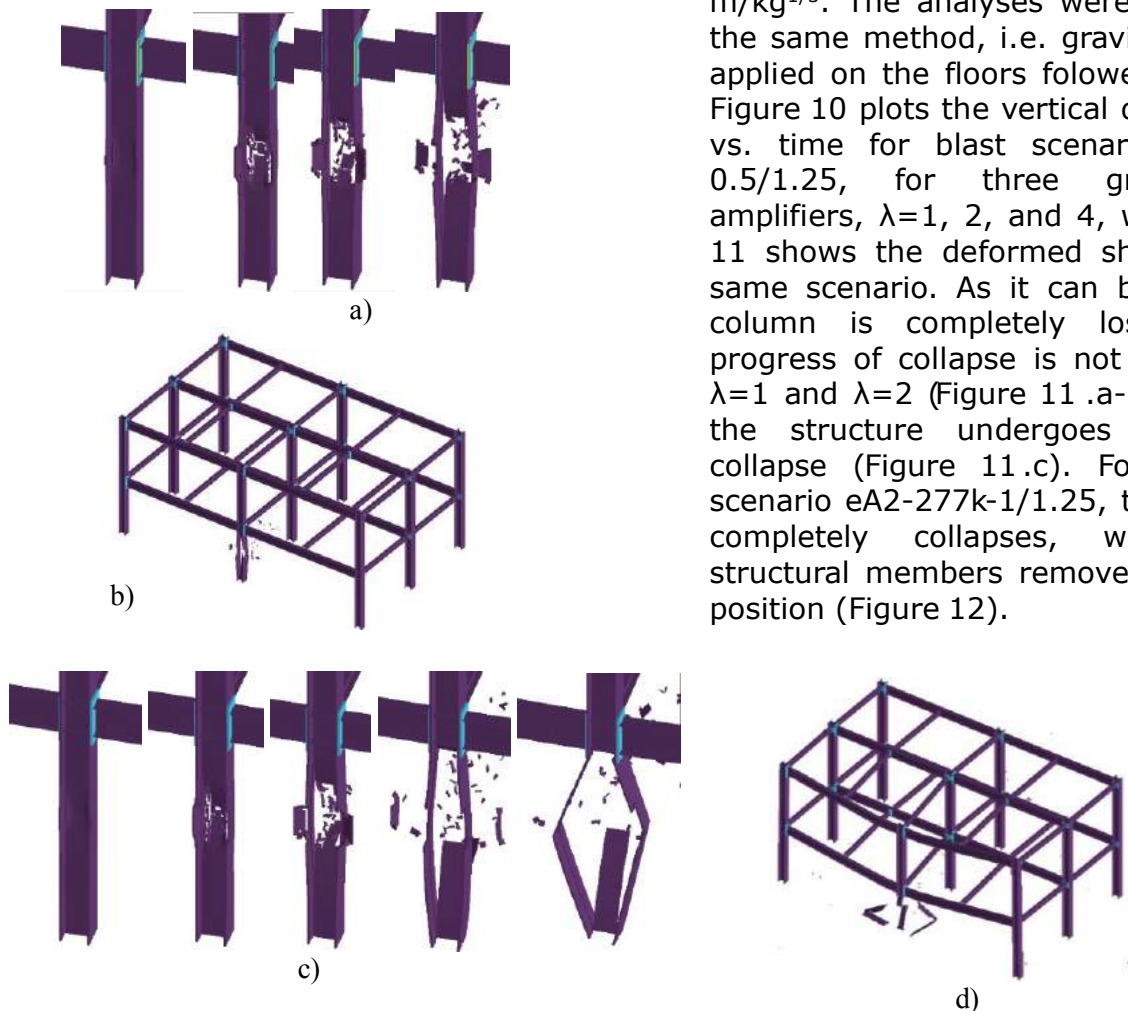


Figure 9. Results for blast scenario eA2-1.8k-0.2/1.25: a) blast damage to column at different moments in time,  $\lambda=1$ ; b) deformed shape,  $\lambda=1$ ; c) blast damage to column at different moments in time,  $\lambda=4$ ; d) deformed shape,  $\lambda=4$

As seen previously, the column is lost for a blast charge of 1815 g at a 0.20 m distance, which results in a scaled distance  $Z = 0.16 \text{ m/kg}^{1/3}$ . Similar blast waves are expected to be produced when two explosive charges with the same scaled distance and similar geometry and explosive, but of different sizes, are detonated in the same atmosphere. However, for a very small standoff distance, the effects can be different. For this reason, two more loading scenarios were considered, i.e. a charge weight of 28.45 kg placed at 0.50 m from the column, and a charge weight of 277.4 kg placed at 1.0 m from the column, respectively. In both cases, the scaled distance is the same, i.e.  $Z = 0.16 \text{ m/kg}^{1/3}$ . The analyses were done using the same method, i.e. gravity loads are applied on the floors followed by blast. Figure 10 plots the vertical displacement vs. time for blast scenario eA2-28k-0.5/1.25, for three gravity load amplifiers,  $\lambda=1, 2$ , and 4, while Figure 11 shows the deformed shape for the same scenario. As it can be seen, the column is completely lost but the progress of collapse is not initiated for  $\lambda=1$  and  $\lambda=2$  (Figure 11 .a-b). For  $\lambda=4$ , the structure undergoes progressive collapse (Figure 11.c). For the blast scenario eA2-277k-1/1.25, the structure completely collapses, with several structural members removed from their position (Figure 12).

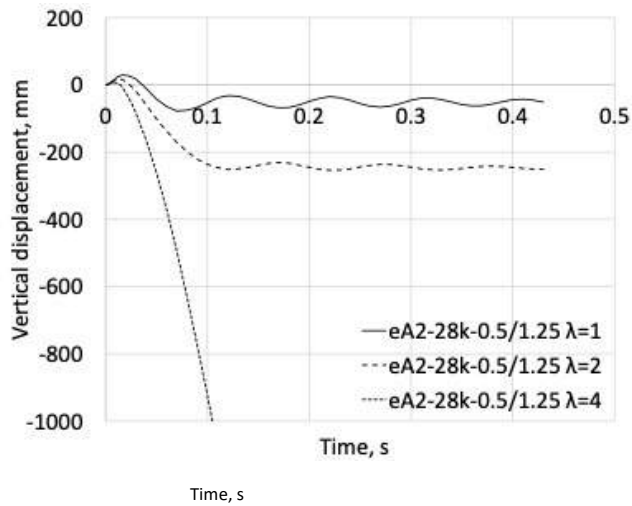


Figure 10. History of vertical displacement for scenario 28k-0.5

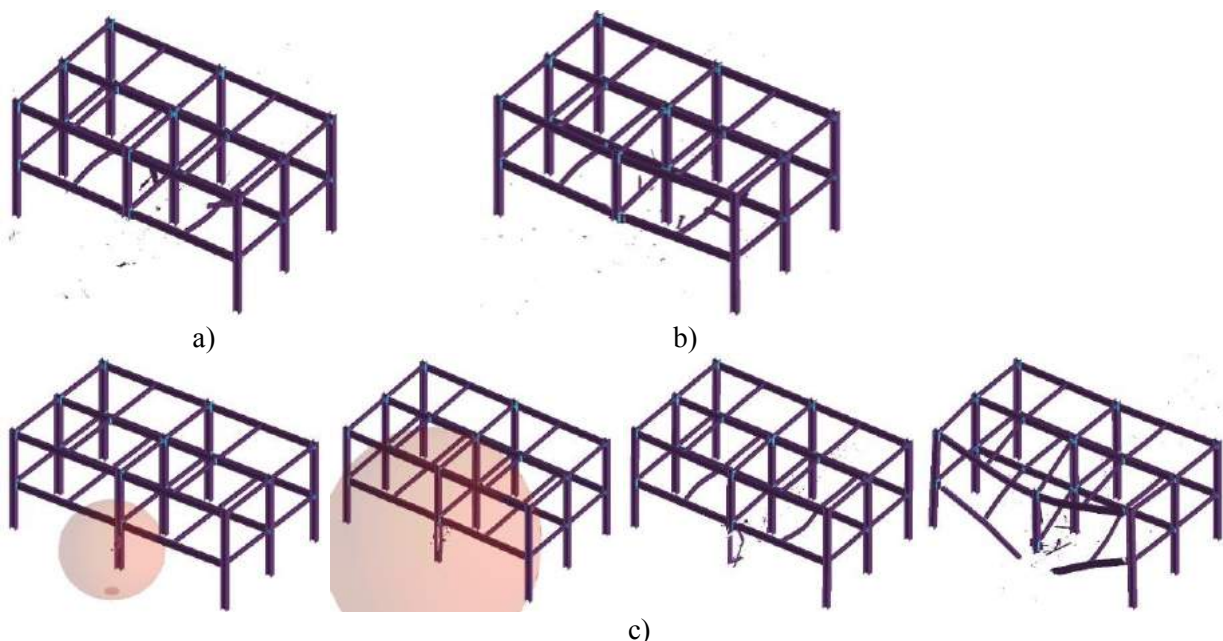


Figure 11. Results for blast scenario eA2-28k-0.5/1.25: a) deformed shape,  $\lambda=1$ ; b) deformed shape,  $\lambda=2$ ; c) deformed shape at different moments in time,  $\lambda=4$

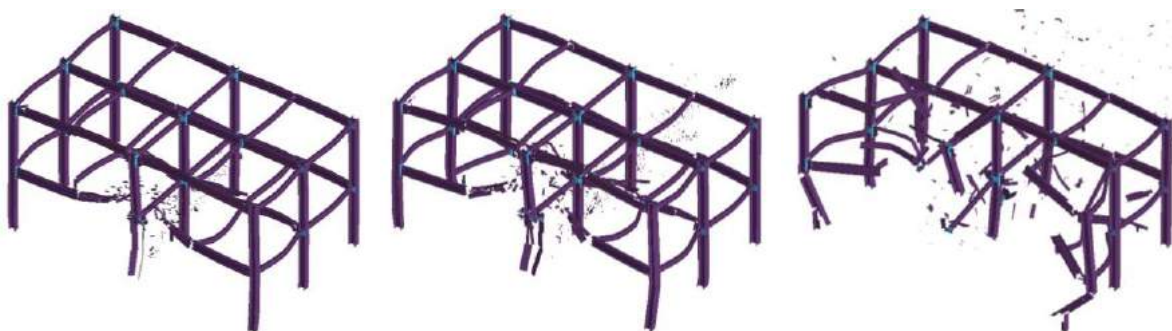


Figure 12. Deformed shape at different moments in time for blast scenario eA2-277k-1/1.25,  $\lambda=1$

Figure 13 compares the vertical displacement curves for scenarios eA2-1.8k-05/1.25 and eA2-28k-0.5/1.25 vs. notional column removal, for two levels of gravity loads, i.e.  $\lambda=1$  and  $\lambda=4$ . As it can be seen, while the 1.8k-02 blast scenario and notional column removal provide similar results, the 28k-0.5 blast scenario leads to larger vertical displacements (for  $\lambda=1$ ) and even collapse (for  $\lambda=4$ ). The larger effects can be attributed to additional damages in members other than the column, but also to the dynamic increase factor. Thus, the upward lift of beams due to direct blast pressure makes the dynamic increase factor go up, with regards to column removal. The pressure wave can “unload” the beams, or even change the sign of the bending moment in the blast phase. The part of the structure subjected to free fall has the same mass for the inertia forces as in the case of notional removal, but also additional forces due to the rebound from the blast pressure (Marginean, 2017). Jahromi et al. (2012) reported a similar behaviour.

## 5. SUMMARY AND CONCLUSIONS

The effects of blast loads can result in the loss of the bearing capacity of a column, or other primary structural members. When placed at a very close distance, even small charges can produce large damages in the members, with the complete fracture of the section walls. In the experimental tests on 3D specimens loaded against the weak axis (blast charge normal to the column web), the punching, or shear-type failure developed, with the web completely separated for a length of almost 600 mm, before the structural element would be able to respond in bending. This case (of column webs directly affected by a blast) is critical, especially for buildings with perimeter steel moment resisting frames and interior gravity frames.

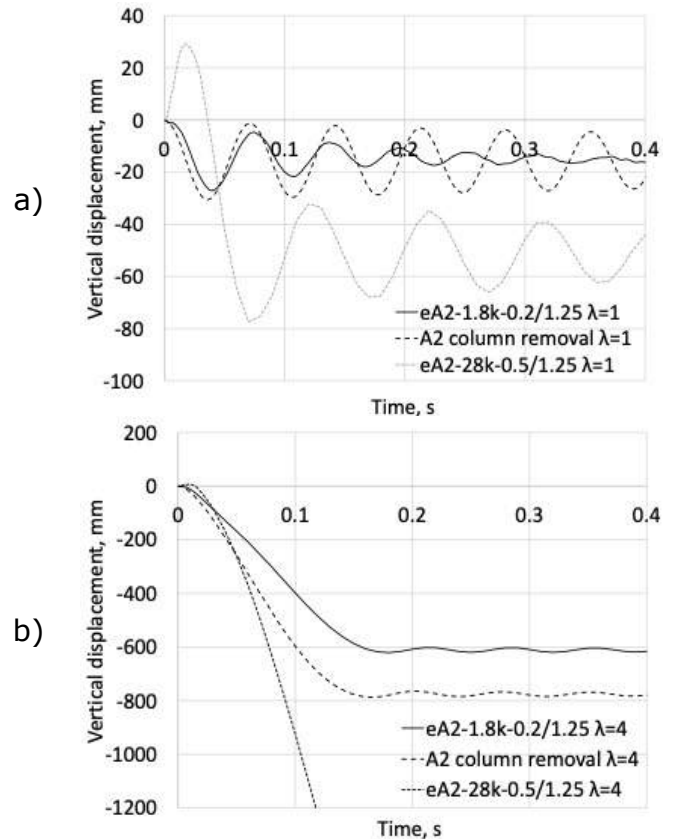


Figure 13. History of vertical displacement for scenarios 1.8k-05 and 28k-0.5 vs. notional column removal: a)  $\lambda=1$ ; b)  $\lambda=4$

Test based calibrated numerical models indicated a very good agreement with the experiment, and were applied to preliminary investigations on a full-scale building structure, using different blast loading conditions. The first blast scenario used a charge weight and distance similar to those used in the experimental tests. For load amplifiers  $\lambda = 4$ , the structure is still stable, without any progression of collapse. Load amplifiers beyond this value will trigger the progressive collapse of the structure. This prediction is important because it will allow the determination of the amount of explosive and the gravity loads that are sufficient to eliminate a column, therefore causing large deflections in the structure, but without the progressive collapse of the entire (or large part) of the structure.

Comparisons were made in terms of structural response between the notional removal of a column and blast loading causing column loss. Due to blast effects on the other elements of the structure and altered dynamic amplification, the vertical displacement of the structure subjected to direct blast can be larger than the vertical displacement resulting in the case of a notional removal.

F. Dinu, D. Dubina  
*Department of Steel Structures and Structural Mechanics, Politehnica University Timisoara, Romania*  
*Laboratory of Steel Structures, Romanian Academy, Timisoara Branch, Romania*

I. Marginean  
*Department of Steel Structures and Structural Mechanics, Politehnica University Timisoara, Romania*

A. Kovacs, E. Ghicioi  
*INCD INSEMEX Petroșani, Romania*

## AKNOWLEDGEMENT

This work was supported by a grant of the Romanian National Authority for Scientific Research and Innovation, CNCS/CCCDI - UEFISCDI, project number PN-III-P2-2.1-PED-2016-0962, within PNCDI III: "Experimental validation of the response of a full scale frame building subjected to blast load" - FRAMEBLAST (2017-2018).

## REFERENCES

- A. Ralston, D. Weggel, M. Whelan & H. Fang, 2015. Experimental and numerical investigations of glass curtain walls subjected to low- level blast loads, *Int. J. Comp. Meth. and Exp. Meas.*, Vol. 3, No. 2 (2015) 121–138.
- Alashker, Y., El-Tawil, S. & Sadek, F. 2010. Progressive Collapse Resistance of Steel-Concrete Composite Floors. *Journal of Structural Engineering* 136(10): 1187-1196.
- ASCE, 2011. Blast protection of buildings. ASCE 59-11 standard, USA.
- Astaneh-Asl, A., Madsen, E.A., Noble, C., Jung, R., McCallen, D.B., Hoehler, M.S., Li, W. & Hwa, R. 2001. Use of catenary cables to prevent progressive collapse of buildings. Report No.: UCB/CEE-STEEL-2001/02.
- Canisius, T.G. 2011. Structural robustness design for practising engineers. COST Action TU0601.
- CEN. 2006. EN1991-1-7: Eurocode 1: Actions on structures – Part 1-7 General actions - Accidental Actions.
- CODEC. 2012. Structural conception and collapse control performance based design of multistory structures under accidental actions (2012-2016). Romania, Executive Agency for Higher Education, Research, Development and Innovation Funding (UEFISCDI).
- CPNI. 2011. Review of international research on structural robustness and disproportionate collapse London, Department for Communities and Local Government
- Cranz, C. 1926. Lehrbuch der Ballistik, Springer-Verlag, Berlin.
- Dinu, F., Dubina, D., Marginean, I., Neagu, C. & Petran, I 2015. Structural Connections of Steel Building Frames under Extreme Loading. *Advanced Materials Research* 1111: 223-228.
- Dinu, F., Marginean, I., Dubina, D. & Petran, I. 2016.a. Experimental testing and numerical analysis of 3D steel frame system under column loss. *Engineering Structures* 113: 59-70.
- Dinu, F., Marginean, I., Dubina, D., Petran, I., Psatrav. M., Sigauan, A. & Ciuatina, A. 2016.b. Experimental testing of 3D steel frame with composite beams under column loss. *In the International Colloquium on Stability and Ductility of Steel Structures*, Timisoara, Romania. 691-698.
- Dinu, F., Marginean, I., Dubina, D., Sigauan, A. & Petran, I. 2016.c. Experimental research on the behavior of steel moment frame connections under column loss scenario. *In Proceedings of the Eighth International Workshop on Connections in Steel Structures*. Boston, USA.
- Dinu, F., Marginean, I., Sigauan, A., Kovacs, A., Ghicioi, E. & Vasilescu, D. 2016.d. Effects of close range blasts on steel frames. Experimental testing and numerical validation. *In the International Colloquium on Stability and Ductility of Steel Structures*, Timisoara, Romania. 699-708.
- DoD. 2014. UFC 4-340-02 - Unified facilities criteria: Structures to resist the effects of accidental explosions. United States Department of Defense, Washington (DC), US.
- DoD. 2016. UFC 4-023-03 - Unified facilities criteria: design of buildings to resist progressive collapse. United States Department of Defense, Washington (DC), US.
- ELS. 2017. Extreme loading for structures (Version 5.0). Durham, NC: ASI-Applied Science International

El-Tawil, S., Li, H. & Kunnath, S. 2014. Computational Simulation of Gravity-Induced Progressive Collapse of Steel-

Frame Buildings: Current Trends and Future Research Needs. *Journal of Structural Engineering*, 140 (8), A2513001

F. Zhang, C. Wu, X. Zhao, H. Xiang, Z. X. L., Q. Fang, Z. Liu, Y. Zhang, A. Heidarpour and J. A. Packer, 2016. Experimental study of CFDST columns infilled with UHPC under close-range blast loading, *International Journal of Impact Engineering*, Vol. 93, July 2016, Pages 184–195.

FRAMEBLAST. 2017. Experimental validation of the response of a full scale frame building subjected to blast load (2017-2018). Romania, Executive Agency for Higher Education, Research, Development and Innovation Funding (UEFISCDI).

Fu, F. 2013. Dynamic response and robustness of tall buildings under blast loading. *Journal of Constructional Steel Research* 80: 299-307.

Hoffmeister, B., et al. 2015. ADBLAST-Advanced design methods for blast loaded steel structures. RFCS-Projekt Nr, RFSR-CT-2010-00 030, 2010-2013.

Hopkinson, B. 1915. British Ordnance Board Minutes 13565.

Kaneko, H. Influence of strain-rate on yield ratio, Kobe Earthquake Damage to Steel Moment Connections and Suggested Improvement, JSSC Technical Report No. 39, 1997.

Karlos, V. & Solomos, G. 2013. Calculation of Blast Loads for Application to Structural Components", JRC 32253-2011 with DG-HOME Activity A5 - Blast Simulation Technology Development, EU, Institute for the Protection and Security of the Citizen.

Kernicky, T.P., Whelan, M.J., Weggel, D.C. & Rice, C.D. 2014. Structural Identification and Damage Characterization of a Masonry Infill Wall in a Full-Scale Building Subjected to

Internal Blast Load. *Journal of Structural Engineering* 141(1): D4014013.

Lukasz Mazurkiewicz, Jerzy Malachowski, Pawel Baranowski, Blast loading influence on load carrying capacity of I-column, *Engineering Structures* 104 (2015) 107–115.

Magallanes, J.M., Martinez, R., Koenig, J.W. 2006. Experimental results of the AISC full-scale column blast test. The American Institute of Steel Construction. Rep. TR-06 20.

Marginean, I. 2017. Robustness of moment steel frames under column loss scenarios. Ph.D. Thesis Department of Steel Structures and Structural Mechanics, Politehnica University of Timisoara.

Mazzolani, F.M. 2010. COST C26. Front Matter. Urban Habitat Constructions Under Catastrophic Events, CRC Press.

Richards, A.B. & Moore, A.J. 2005. Blast vibration course measurement - assessment - control. Terrock Pty Ltd.

Sadek, F., El-Tawil, S. & Lew, H.S. 2008. Robustness of composite floor systems with shear connections: Modeling, simulation, and evaluation. *Journal of Structural Engineering* 134(11): 1717-1725.

Song, B.I, Giriunas, K.A. & Sezen, H. 2014. Progressive collapse testing and analysis of a steel frame building. *Journal of Constructional Steel Research* 94: 76-83.

Tagel-Din, H. & Meguro, K. 2000 Applied element method for simulation of nonlinear materials: Theory and application for RC structures. *Structural Engineering/Earthquake Engineering, International Journal of the Japan Society of Civil Engineers (JSCE)*, 17: 137-148.

Yang, B. & Tan K.H. 2013. Robustness of bolted-angle connections against progressive collapse: Mechanical modelling of bolted-angle connections under tension. *Engineering Structures* 57: 153-168.

Zolghadr, J.H., et al. 2012. Robustness Assessment of Building Structures under Explosion. *Buildings* 2(4): 497-518.

EFEE Booth  
26 & 27

**finexplo**

web: [www.finexplo.fi](http://www.finexplo.fi)  
tel. +358 40 544 3656  
info@finexplo.fi

**AUTOSTEM**  
AutoStem Gen3

**SHOTTRACK**  
make every shot count

Track & Trace **IIE**  
Europe GmbH

**ROTHENBUHLER ENGINEERING**

**EXPLOSION**

# BLASTANE

High purity hydrocarbon  
fluids for Ammonium  
Nitrate explosives

BLASTING  
RESPONSIBLY



[www.totalspecialfluids.com](http://www.totalspecialfluids.com)



**TOTAL**

Committed to Better Energy



## **Cloud scanning and photogrammetry – a comparison of blast face surveying techniques**

**ABSTRACT:** The use of unmanned aerial vehicles (UAV), more commonly referred to as 'Drones', has significantly increased on a global basis in recent years. In the mining and quarrying sector, drone mounted cameras combined with photogrammetry software can facilitate the rapid production of 3-D models of excavations from a blast face to whole pits, significantly reducing the time and expense of traditional surveying and scanning techniques. To assess the comparative performance of these techniques, a quarry face was captured and modelled using drone based and hand-held camera images alongside traditional laser based face profiling techniques. These models were then compared to a baseline scan of the same face acquired using a cloud scanner, and the differences assessed in 3-D to provide guidance on the relative accuracies of each technique and to demonstrate the viability of photogrammetry in face profiling applications.

## 1. INTRODUCTION

The use of unmanned aerial vehicles (UAV), more commonly referred to as 'Drones', has increased dramatically in recent years. Improvements in technology have reduced their complexity and cost, promoting their accessibility in both the commercial and recreational sectors.

In mining and quarrying, the application of drones equipped with high resolution cameras can contribute to operations in a range of areas from assisting with inspections and photographic records to rapid generation of full 3-D models of excavations when combined with the latest photogrammetric software.

The underlying technique of photogrammetry offers a simple, fast and efficient way to obtain survey data with significantly lower entry costs than conventional survey equipment. The technique is not just confined to drones, and can be undertaken using every day hand-held cameras, allowing surveys to be conducted in conditions and areas where drone flights are not possible including where there are airspace restrictions and poor weather.

Several comparisons have previously been made between drone based surveys and conventional face profiling techniques, for example in Wiegand & Valentim (2016) and Moser *et al.* (2007), which have generally indicated a high degree of accuracy.

As part of their ongoing research into the use of drones for blast and quarry survey applications, the authors set out to undertake their own assessment of the techniques accuracy applicable to face profiling by comparing 3-D models formed from drone and hand-held camera images and those obtained from conventional face profiling techniques. To provide an accurate baseline for comparison, the authors carried out a high-density cloud scan of the face from which the differences measured to the photogrammetry and laser profiler derived models were assessed.

## 2. PHOTOGRAMMETRY PROCESS

Stereo-photogrammetry, often abbreviated to photogrammetry, matches a series of common points between 2 or more photos of an object taken from different positions and angles and uses software algorithms to determine each image's camera position. From these derived camera positions, the 3-D position of all other common points in the images can be determined and a 3-D model formed as described in Birch (2010)

By incorporating targets into the models with known points, these models can be georeferenced allowing each point's real-world coordinate to be determined.

## 3. METHODOLOGY FOR COMPARISON OF ACCURACY

To assess the relative accuracy of the different surveying techniques, a common face was selected for modelling using each of the identified methods. An approximate 60 m length by 20 m height face of Kaolonised Granite was selected in a surface mine as shown in Figure 1. This face was chosen as it contained multiple protruding features which would help to assess the ability of the different survey techniques to capture complex shapes.

To allow the face to be georeferenced, a series of 3 painted targets were placed on the lower bench in front of the face, with 3 further targets placed on the upper bench which were visible from above only. These targets positions were recorded using the site GPS. In addition, a total of 6 smaller radial targets (not georeferenced) were placed along the lower bench for use by the cloud scanner to aid joining of the scans. A diagram of the target setup is shown in Figure 2.



*Figure 1. Surveyed face.*

Survey Method	Number of setups	Point spacing
High definition cloud scan	3	Approx. 25 x 25mm at face
Laser profiler 1	3	100 x 100 mm auto adjusted for distance
Laser profiler 2	3	100 x 100mm auto adjusted for distance
Drone based camera	104 (images)	-
Hand-held camera	40 (images)	-
Camera phone	19 (images)	-

*Table 1. Survey methods.*

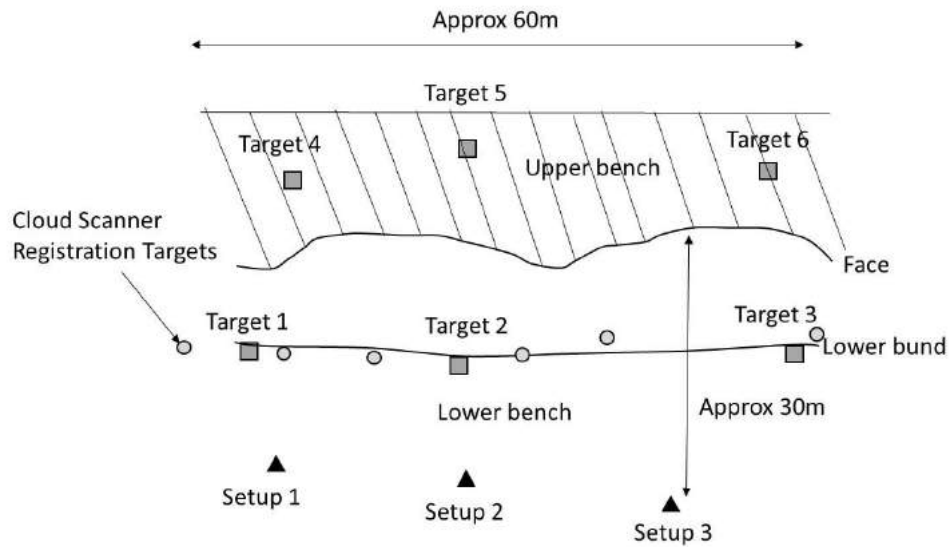


Figure 2. Target layout.

A total of 6 different surveys were undertaken. The high definition cloud scanner utilised in the trial was a Leica ScanStation C10 which can produce a 3-D point position accuracy of 6mm at 50m. The drone utilised was a DJI Phantom 3 Professional with a gimbal mounted camera which acquired images at 12 megapixel resolution. The hand-held camera had a 20 megapixel resolution and the camera phone a 13 megapixel resolution.

For the cloud scanner and laser profilers, each was setup at 3 different positions in front of the face as previously shown in Figure 2.

For the hand-held camera and camera phone, images perpendicular to the face were taken at an approximate 5m spacing offset at 20 m as indicated in Figures 3 and 4.

For the drone, this was operated manually with images taken in an approximate 5m x 5m horizontal grid looking vertically downwards 20m above the bench top covering the bench area. After this, 6 more passes of decreasing elevation were made in front of the face with the camera orientated downwards at -45 degrees pitch, perpendicular to the face and towards the face and upwards at +45 degrees pitch followed by a final low pass looking vertically downwards behind the lower bund as indicated in Figure 5.



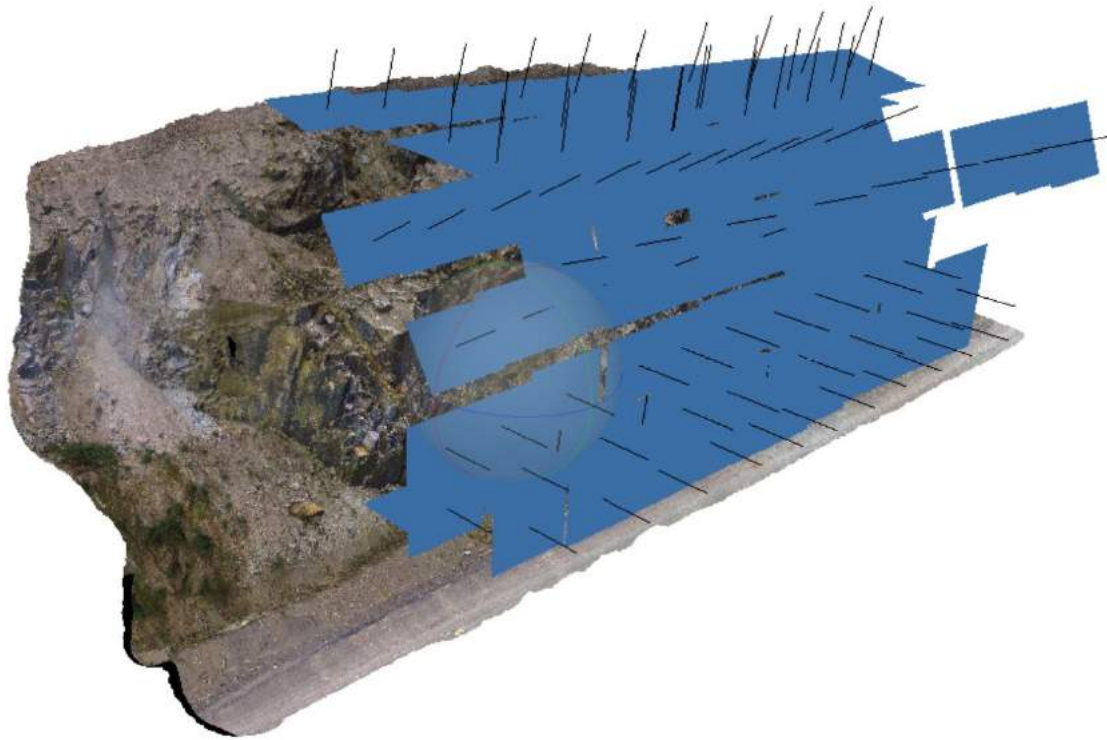


Figure 5. Drone image locations.

#### 4. COMPUTER MODELLING

For a comparison to be made, point clouds first needed to be generated for each set of data from the different techniques. For the high definition cloud scan, the scans acquired from each of the setup positions were merged in the scanner software using the radial targets as common points. The merged cloud was then georeferenced using the painted target coordinates on the lower bench only as the upper bench ones were not visible.

For the laser profilers, the data from the 3 setups for each scanner was merged using each individual scanner's accompanying software with points already georeferenced from the profiler setup positions that were picked up by the GPS survey.

For the drone, hand-held and camera phone images, these were imported and processed in an industry standard photogrammetry software package to form a dense point cloud. The drone model was georeferenced to both the lower and upper targets due to its ability to see both the upper and lower bench, whilst the hand-held camera and camera phone images were georeferenced using the bottom 3x targets only as these were the only ones visible.

After generation of the point clouds, all data was exported in an XYZ format and imported into CloudCompare, an open-source direct cloud comparison software package. The cloud scanner point cloud was imported as a mesh to act as the baseline whereas the other models were imported as a raw point cloud. A common viewpoint of approximately 15 m height by 65 m width was setup looking directly at the face and the points cloud models trimmed to a common size with the baseline cloud scanner mesh extending approximately 1 m on all sides to ensure overlap.

The software then analysed the difference from the baseline cloud scan mesh to each point cloud by measuring the distance between each point in the cloud and the nearest interpolated point on the baseline mesh. CloudCompare then output a colour map of the face showing the distribution of errors as well as a histogram to which a Gaussian Distribution is fitted.

A summary of the distribution of errors relative to the cloud scanner model is shown in Table 2.

Model Name	Mean Error (m)	Standard Deviation (m)	Number of Photos	Number of Points in Point Cloud	Notes
High definition cloud scan	-	-	-	1,691,234	0.1 m Grid at 100 m, approx. 25 x 25 mm on face
Drone based camera	-0.00108	0.02160	104	998,735	All photos employed. Georeferenced using top and bottom targets.
Laser profiler 1	0.01342	0.0472	-	108,955	0.1 m Grid on face
Laser profiler 2	-0.01600	0.06537	-	178,651	0.1 m Grid on face
Hand-held camera	0.03310	0.0966	40	1,522,038	All photos employed. Georeferenced using bottom targets only.
Camera phone	0.12710	0.3253	19	1,167,754	All photos employed. Georeferenced using bottom targets only.

Table 2. Summary of model errors.

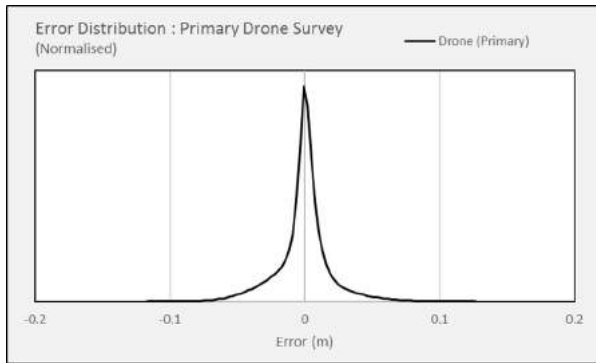


Figure 6. Drone based camera distribution of errors.

Due to the different number of points in each model and variable bin sizes in the exported histogram, the error data was normalised allowing a direct comparison of the error distribution from the cloud scanner model for each survey method. These are shown in Figure 6 for the 'Drone based camera' model, and Figure 7 to Figure 10 for the other methods overlay with the drone model for comparison.

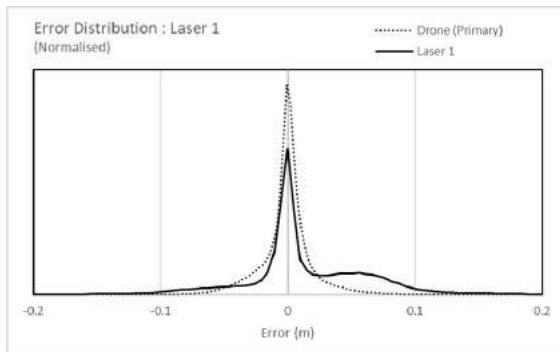


Figure 7. Laser profiler 1 distribution of errors.

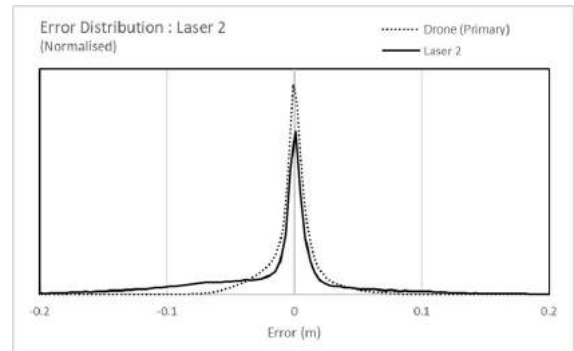


Figure 9. Hand-held camera distribution of errors.

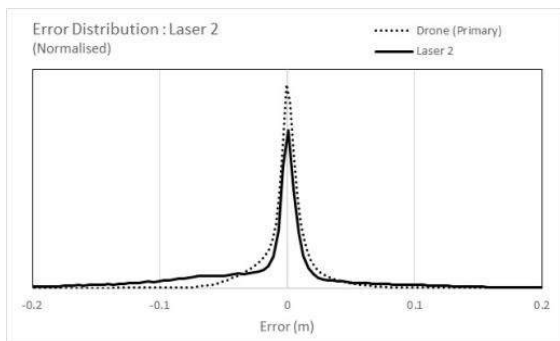


Figure 8. Laser profiler 2 distribution of errors.

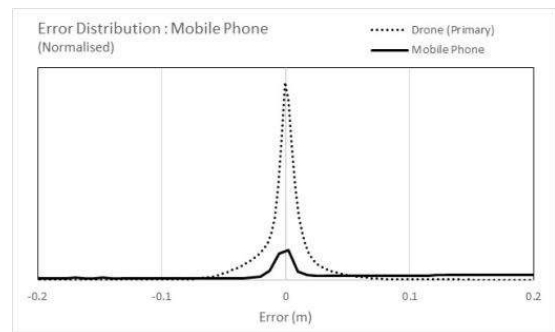


Figure 10. Camera phone distribution of errors.

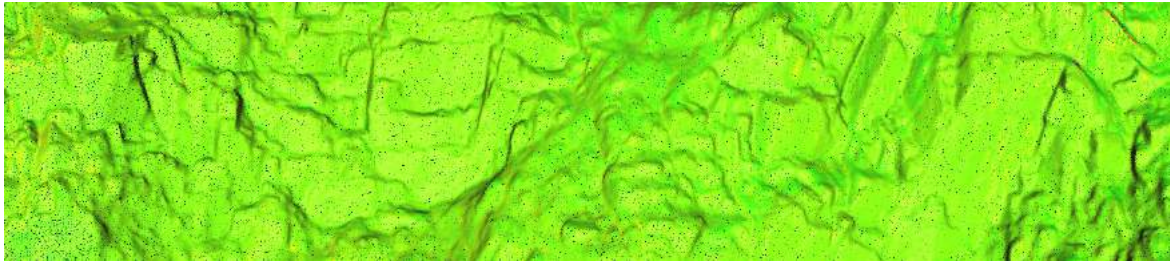


Figure 11. Difference map for the drone model.

## 5. MODEL COMPARISONS

Assessing the calculated mean errors and their standard deviations shows that the drone camera model was the closest to the cloud scanner model with a mean error of approximately 1mm and a standard deviation of approximately 22 mm. Analysing the colour map for the location of these errors as shown in Figure 11 did not indicate any concentrations of errors at a particular location. This suggested that the drone model was sufficiently constrained about its reference points and that the large number of photos utilised in this technique helped to ensure that major features were accurately modelled.

Note in Figure 11: Darker areas represent the greatest variation and black areas represent areas where there were no points modelled).

Both laser profilers produced comparable results with a mean error of 13 and 16 mm respectively though a slight skewness was seen in both models suggesting a difference in the relative orientation of the two scans to the cloud scanner model. It was considered that this was due to a slight variance in the pickup of the reference targets which were used to orientate the face profilers during setup.

The hand-held camera and camera phone image models performed least well with a mean error of 33 mm and 127 mm respectively and a negative skew visible in both cases as demonstrated by the greater proportion of positive errors. Assessing the colour maps for the locations of these errors as shown in Figures 12 and 13, it was apparent that these errors were predominately concentrated along the top of the scan alongside several areas where no surface could be modelled. This location suggested that the two models

were not sufficiently constrained vertically as neither upper bench or top targets were visible, resulting in a slight rotation of the model in comparison to that obtained by the drone. In addition, the areas where no surface could be modelled suggested that the greater number of photos taken by the drone and its different vantage position had aided the modelling process allowing it to form a more representative model.

To investigate the impact of the upper vantage positions gained by using the drone, a separate model using the drone images was created, georeferenced using the bottom targets only, to mimic the control used in the hand-held and camera phone models. In addition, to assess the impact of the number of photos acquired by the drone, it was also decided to also generate models using  $\frac{1}{2}$  and  $\frac{1}{4}$  of the total photos captured by the drone, georeferenced using both the bottom and top targets. The results of these additional analyses are shown in Table 3 with the histogram distribution of errors shown in Figures 14 to 16 respectively.

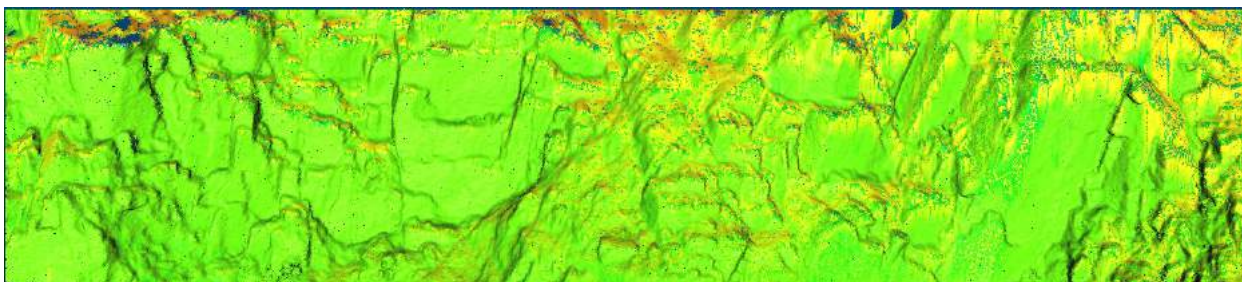


Figure 11. Difference map for the drone model.

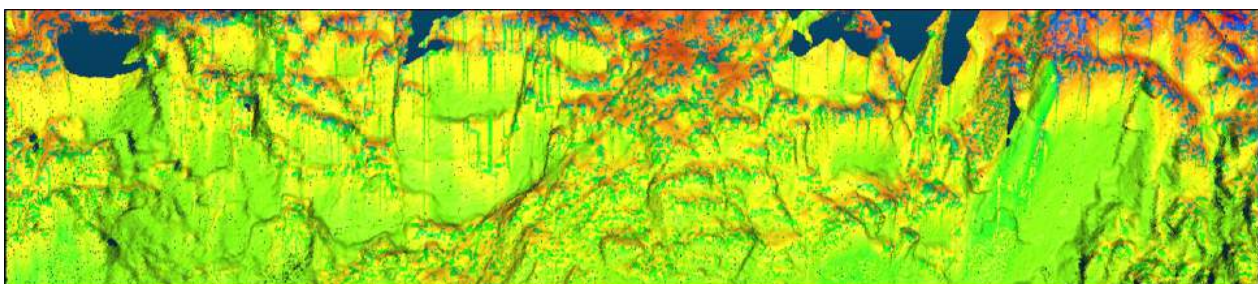


Figure 12. Difference map for the hand-held camera.

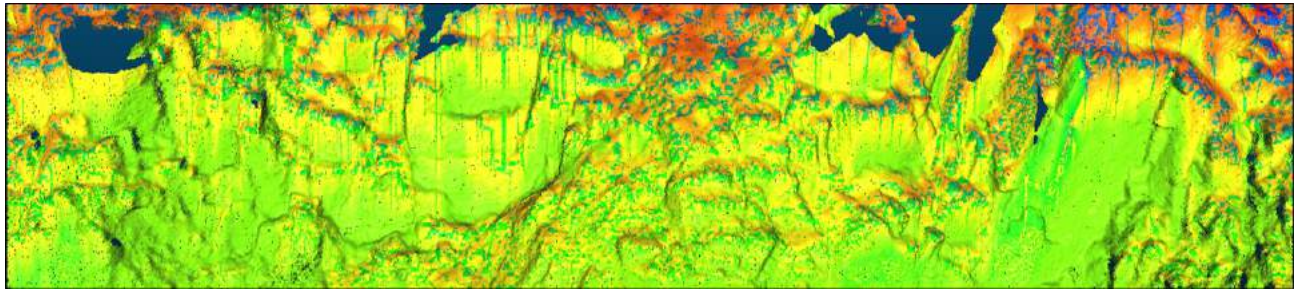


Figure 13. Difference map for the camera phone

Model Name	Mean Error (m)	Standard Deviation (m)	Number of Photos	Number of Points in Point Cloud	Notes
Drone based camera Bottom Targets Only	0.04287	0.11476	104	986,296	All photos employed. Georeferenced using bottom targets only.
Drone based camera 1:2	0.00091	0.01775	57	937,860	1 in 2 photos employed. Georeferenced using top and bottom targets.
Drone based camera 1:4	0.00174	0.02187	29	815,285	1 in 4 photos employed. Georeferenced using top and bottom targets.

Table 3. Summary of drone model errors.

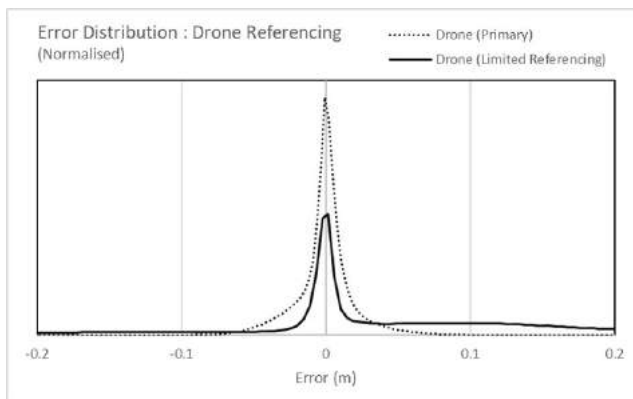


Figure 14. Drone based camera distribution of errors (bottom targets only).

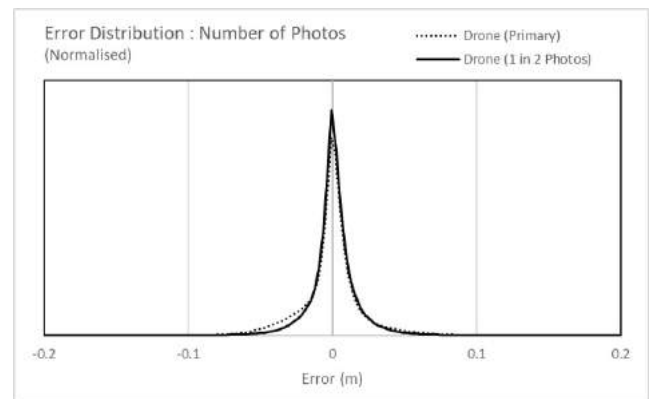


Figure 15. Drone based camera 1:2 distribution of errors.

As shown in Figure 14, when utilising the bottom targets only to reference the drone model, the mean errors and standard deviation increased with a negative skewness shown, again indicating that the model was not sufficiently constrained vertically as also seen in the error distribution map shown in Figure 17.

The reduced subsets of photos shown in Figures 15 and 16 produced similar errors to that of the main drone model however, on inspection of the error distribution map for these models, it was noted that when using the 'Drone based camera 1 : 4' model, the proportion of the surface that could not be modelled increased as shown in Figure 18.

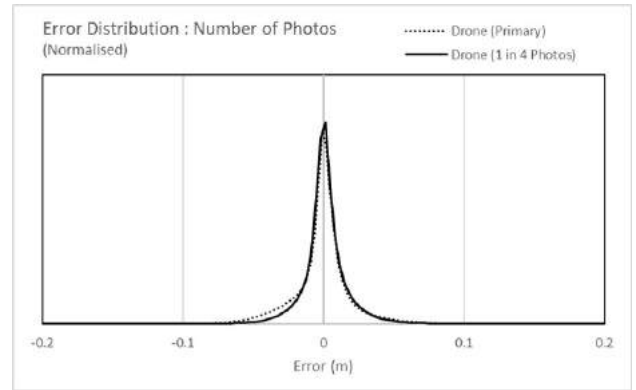


Figure 16. Drone based camera 1:4 distribution of errors.

The above analysis demonstrates the advantage of using the drone to acquire images over hand-held cameras. The increased number of photos provided by the drone significantly improved the modelling process and its ability to capture detail from the upper bench and top targets helped to better form and constrain the model in these areas.

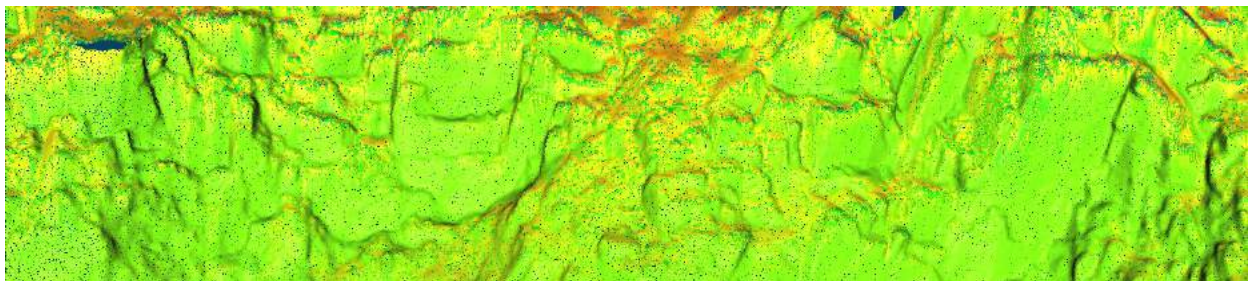


Figure 17. Difference map for the drone based camera model with bottom target referencing.

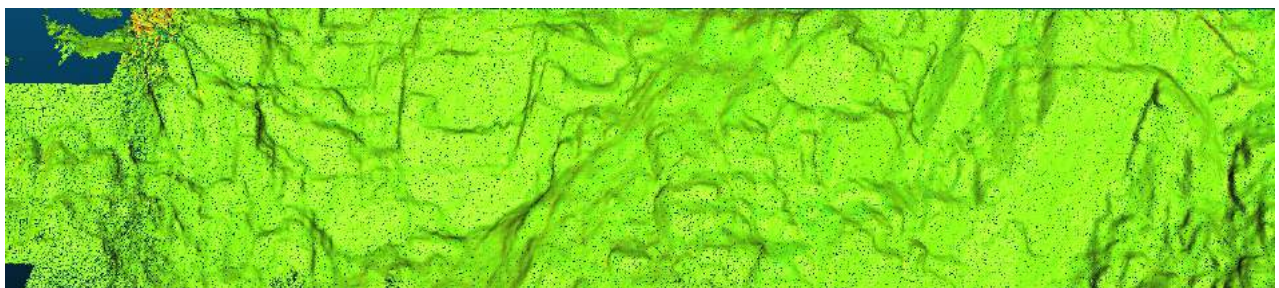


Figure 18. Difference map for the drone based camera 1:4 model.

## 6. CONCLUSIONS

Based on the analysis of a drone image derived photogrammetry model of a quarry face, the technique was found to produce comparable results to that of scans from a high definition cloud scanner and to that from traditional laser profile survey techniques when a sufficient quantity of photos was obtained from multiple vantage points.

Further analysis using hand-held and camera phone obtained images highlighted the sensitivity of the technique to misalignment if insufficient reference targets are used in the vertical domain. When using these methods, it was found that the formed models were rotated in the vertical axis leading to errors on the upper edges of the face. This suggests that when using hand-held methods, additional targets on the upper bench that are visible from the lower bench are required to enable it to be sufficiently constrained.

*G. Adderley, S. Bolitho,  
R. Farnfield, & A. B. Keverne  
Wetherelt*

*EPC United Kingdom Plc, Alfreton,  
Derbyshire, United Kingdom, Imerys  
Minerals Ltd, St Austell, Cornwall,  
United Kingdom, Camborne School of  
Mines, University of Exeter, Penryn,  
Cornwall, United Kingdom*

Use of the drone was also found to assist in the overall ability of the software to model the whole face. When using the hand-held and camera phone images, a higher proportion of the face was unable to be modelled suggesting that the additional image orientations gained by using the drone provided better coverage of features on the face.

Use of the drone offered a fast and efficient way to acquire a representative survey of a quarry face taking about 15 minutes to conduct the survey and 30 minutes to process the model. Whereas the other techniques utilised in the trial captured just the quarry face from their positions on the lower bench, the drone was also able to acquire images and model the upper bench which combined with the low average error compared to the cloud scan demonstrated the viability of the technique when properly applied.

## REFERENCES

Birch, J. 2010. How does photogrammetry work? Belmont: ADAM Technology (online). Available from: <http://www.adamtech.com.au/Blog/?p=102> (Accessed 30 April 2017).

Moser, P. Ganster, M. & Gaich,

A. 2007. Experience with and benefits from the use of 3-D stereophotogrammetry for blast design and control. *In: Proceedings of the 33<sup>rd</sup> Annual Conference on Explosives and Blasting Technique, Nashville 28 - 31 Jan 2007.* Cleveland: International Society of Explosives Engineer.

Wiegand, J.E. & Valentim, L. 2016. Using photogrammetry data from unmanned aerial vehicle (UAV), small unmanned aircraft systems (sUAS) for blast design. *In: Proceedings of the 42<sup>nd</sup> Annual Conference on Explosives and Blasting Technique, Las Vegas 31 Jan - 4 Feb 2016.* Cleveland: International Society of Explosives Engineers.



**Formulated for your success.**

Uphole bulk emulsion charging is challenging when using typical emulsion explosives.

Lubrizol® Uphole technology is an easy-to-use shear-thickening emulsifier product that can formulate the desired viscosity at the point of hole charging. Ready to use with your current mixing and pumping equipment, Lubrizol Uphole emulsion can be pumped through a shearing nozzle to increase viscosity while minimizing emulsion crystallisation.

Contact your Lubrizol account manager to learn more.

**ADEX**  
Emulsifiers

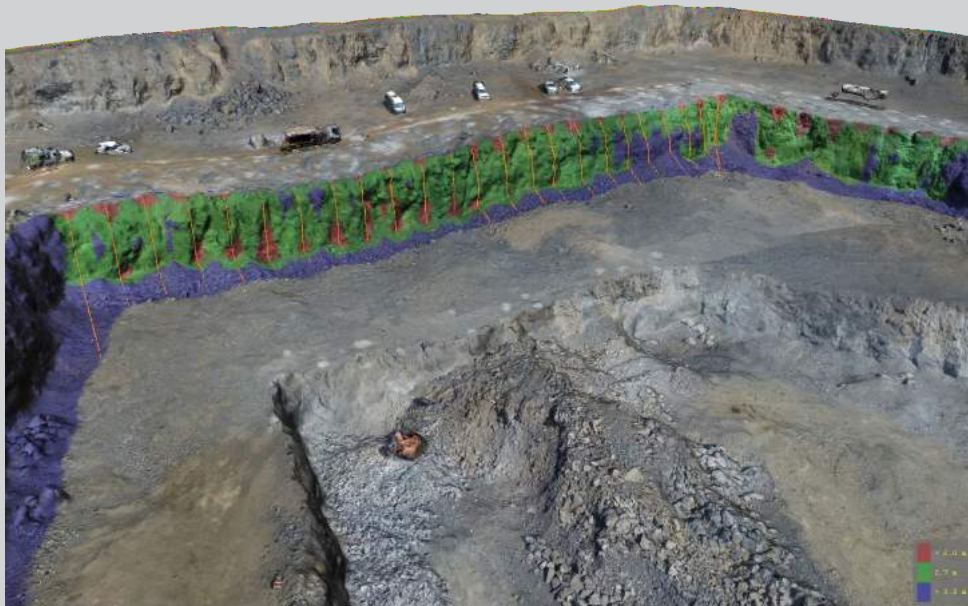
The Lubrizol Corporation  
[www.lubrizol.com](http://www.lubrizol.com)

**Lubrizol**

# BlastMetriX UAV

## Aerial 3D imaging

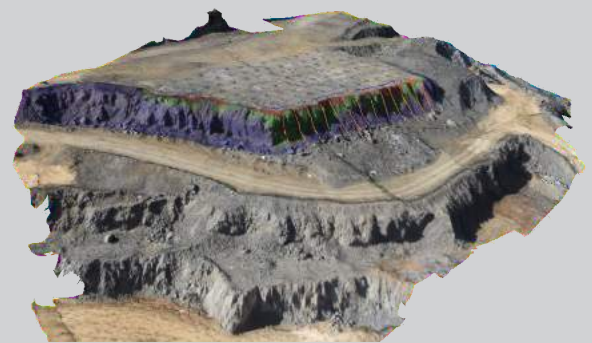
Blast Design and Blast Analysis with 3D images



3D images from drones are a perfect survey of large blast sites. Poor blasting results are often caused by inaccuracy of the front row hole placement and suboptimal blast pattern geometry.

### Features

- Face profiles (burden diagrams and maps)
- Volume to blast
- Pre-post blast comparison
- Quantification of muckpile (movement, volume, swell)
- Power trough
- Seamless data flow



**3GSM**  
Software & Measurement  
3GSM.at

3GSM GmbH  
8010 Graz - Austria  
office@3gsm.at - www.3GSM.at

## PECCS - Multiplier Event in Berlin



It has been almost three years since the beginning of the PECCS project. The goals of this project have always been big and the hopes are still high. With this project we not only want to harmonize the shot firer educational levels in Europe, we also wish to make the education more available in all countries in Europe. With very big goals, three years is a short time, but already now, we can say that we have done what we planned to and we can move forward towards our dreams. On 27th March in Berlin we had reason to celebrate, or it can also be called the Multiplier Event, which was created in order to share the PECCS ideas and show what we have done so far for the shot firer education.

The event was visited by more than 50 people, most of them were teachers and trainers of shot firer, but also authorities from different European countries.

All the PECCS ideas were introduced by the project partners but also by the representative of the EFFE Board. All 8 chapters: the Explosives, Blasting Close to Existing Structures and Contour Blasting, Tunneling, Blasting Geology, Initiation Systems, Blasting Theory, Drilling and Machinery and Safety were summarized to show what levels we have and how this course could help the explosives and blasting industry.

During lunch and coffee breaks people shared experiences with difficulty of the shot firer mobility and the differences of this profession in European countries has been acknowledged for a long time now that something needs to be done.

Surely, there's still few more months to go, and then we have to report the outcomes of the project to the European Commission. But our motivation is very high, as we have had very positive feedback from the Multiplier Event participants. Here is a cut from an open opinion from Germany:

"I found the presentation particularly interesting, because we are in a need to understand, how trained blasting experts can be accepted in Germany, when they come from other countries and wish to work in Germany. The (almost) free movement of work power in Europe is an important principle.

The knowledge of the legal conditions and the national laws applicable to blasting operations will always stay an issue, which requires a national solution. By solution I mean teaching program, tests, licenses. But the more technical part, and also regarding safety of operations, this should be a common base in Europe.

I think it is more efficient, and also safer in terms of coverage and up-to-date information, when the technical parts of a blasters training are unified throughout Europe.

Currently such a program, as you presented it in the PECCS multiplier event is not yet part of training in Germany. And several questions remain to be resolved, e. g. how national laws and technical information interlock.

After having seen the good quality of the information shown at the PECCS multiplier event, I feel very encouraged to follow up on this matter and to seek contact with people in Germany, how one could move forward.

Thank you to you and your colleagues for organising this interesting event."

EFEE is planning to take this course and put it into action this autumn 2019, after the project has ended. To do this, we are looking for cooperation initiatives from educational entities all over Europe. The materials are free of charge and the education must have a wide reach. The Pan-European Competence Certificate for Shot-firers will not be finished with just this project, but it will always keep developing and we will always keep in mind the benefits of the industry and the workers first hand.

We do not wish to change any regulations or laws in any country and we are always open to give a hand where support is needed with educational enhancement.

*Teele Tuuna - PECCS project technician, shot-firer*



*PECCS project partners in Berlin*

# The art of successful blasting



**Nitro Consult**  
www.nitroconsult.se

# INFRA

A complete solution for remote construction site monitoring

 **Blast application available**

**INFRA Net** | Sigicom

Dashboard | Projects | Data reports | Messages | Hardware | Users

Project: Blasting Stockholm

Project ID: 20131002 | Project name: Blasting Stockholm | Project time frame: 2013-10-02 15:00 - 2015-12-31 00:00 | Time zone: Europe/Stockholm

Customer: | Customer contact: | Project maintainer: | Blast standard: SS434065

Measure points | Blast events | Map | Users

Unplaced

Linear regression analysis

sigicom.com



**Sigicom**

## **New EFEE Members**

EFEE likes to welcome the following members who recently have joined EFEE.

## **Individual Members**

Frédéric Monath, BOUYGUES TP / Mining Division (DTP Mining), France

Peter Schimek, VA Erzberg GmbH, Austria

## **Corporate Members**

HANWHA CORPORATION, Seoul, South Korea

Epiroc Rock Drills AB, Örebro, Sweden

## **Upcoming International Events**

EFEE 10<sup>th</sup> World Conference on Explosives and Blasting

September 17-19, 2019

Helsinki, Finland

[www.efee2019.com/](http://www.efee2019.com/)

International Congress on Rock Mechanics and Rock Engineering

September, 13-18, 2019

Foz do Iguassu, Brazil

<http://www.isrm2019.com>

ISEE 46th Annual Conference on Explosives and Blasting Technique

January 26-29, 2020

Denver Colorado, USA

<https://www.isee.org/conferences/2020-conference>

SME Annual Conference

February 23-26, 2020

Phoenix, Arizona USA

[www.smeannualconference.com](http://www.smeannualconference.com)

WORLD TUNNEL CONGRESS 2020

May, 15-21, 2020

Kuala Lumpur, Malaysia

[www.seacetus2017.com/4/443/welcome-to-malaysia/](http://www.seacetus2017.com/4/443/welcome-to-malaysia/)

SAFEX International Congress #20

May 27-29, 2020

Salzburg, Austria

<https://iexpe.org/safex-congress-bulletin-call-papers/>

EUROCK 2020

June, 15-19, 2020

Trondheim, Norway

<http://www.eurock2020.com/hjem.cfm>

SME Annual Conference

February 28-March 3, 2021

Denver, CO, USA

[www.smeannualconference.com](http://www.smeannualconference.com)

World Mining Congress

July 20-22, 2021

Brisbane, Australia

[www.wmc2021.org](http://www.wmc2021.org)

## Upcoming National Events

Informationstagung für Bohr-, Spreng- und Ankertechnik

Place: CAMPUS SURSEE Bildungszentrum Bau, CH-6210 Sursee LU, Switzerland

Date: 13. / 14. September 2019

Official language: German

Website/Contact info regarding the conference: [www.sprengverband.ch](http://www.sprengverband.ch)